UNIVERSITY OF NOVA GORICA

SCHOOL OF APPLIED SCIENCES

CHEMICAL AND STRUCTURAL INVESTIGATION OF THE COBALT PHTHALOCYANINE

MASTER THESIS

Matija Stupar

Mentors:

doc. Dr. Barbara Ressel

prof. Dr. Giovanni De Ninno

Nova Gorica, 2015

UNIVERZA V NOVI GORICI

FAKULTETA ZA APLIKATIVNO NARAVOSLOVJE

KEMIČNA IN STRUKTURNA RAZISKAVA MOLEKULE KOBALTOVEGA FTALOCIANINA

MAGISTRSKA NALOGA

Matija Stupar

Mentorja:

doc. dr. Barbara Ressel

prof. dr. Giovanni De Ninno

Nova Gorica, 2015

Acknowledgements

I would like to thank my mentors, doc. Dr. Barbara Ressel for her guidance, patience, numerous learning lessons, and for having introduced me to the field of materials research, and Prof. Dr. Giovanni De Ninno for his help, valuable suggestions and opportunities.

I would also like to thank Prof. Carla Puglia and Teng Zhang, from University of Uppsala, for letting me join the experiments at Gas Phase. Big thanks goes also to Dr. Marcello Coreno, for "hosting" me and sharing his knowledge on hemispherical spectrometers and experimental techniques during the beamtime. I cannot forget Dr. Monica De Simone, Dr. Cesare Grazioli and Dr. Maddalena Pedio from Gas Phase and CNR-IOM for extensive explanations during the experiments and help in the process of data analysis.

For providing a precious insight into strengths and weaknesses of the density functional theory, I would like to thank doc. Dr. Layla Martin Samos.

Last but not least, I would like to thank my parents for support, and my girlfriend Ana for patiently postponing all holiday plans to winter.

Povzetek

Organske molekule, ki so po sestavi podobne ključnim molekulam v naravi, kot sta klorofil ter hemoglobin, so v zadnjih letih pritegnile pozornost raziskovalcev. Omenjene molekule so gradniki materialov, ki jim pravimo tudi organski polprevodniki. Njihova uporaba sega na mnoga področja, npr. od naprav za shranjevanje podatkov do sončnih celic. Nekatere izmed prednosti the materialov so nizka cena, nizka teža, preprost inženiring in mehanska upogljivost, ki omogočajo njihovo uporabo na upogljivih plastičnih substratih.

V magistrski nalogi bodo predstavljeni rezultati raziskav kemičnih, strukturnih in elektronskih lastnosti kobaltovega ftalocianina; ta molekula je zaradi feromagnetnih lastnosti kobaltovega atoma še posebej zanimiva za uporabo na področjih magnetnega shranjevanja podatkov in spintronike. Pri raziskavah lastnosti kobaltovega ftalocianina v plinastem stanju, t. j. v odsotnosti interakcij z okolico, so uporabljene tehnike, kot sta fotoemisijska spektroskopija notranjih in valenčnih elektronskih stanj ter rentgenska absorpcijska spektroskopija. Lastnosti molekul so bile preučevane v visokem vakuumu.

Preostali poskusi, ki so predstavljeni v nalogi, so bili namenjeni karakterizaciji novega svetlobnega vira CITIUS, ki ga bomo v prihodnjih raziskavah uporabljali za časovno odvisne fotoemisijske meritve na molekulah kobaltovega ftalocianina na površinah.

Ključne besede: kobaltov ftalocianin (CoPc), fotoemisijska spektroskopija (PES), roentgenska absorbcijska spektroskopija (XAS), sinhrotronska emisija, laser, generacija visokih harmonikov, časovno odvisna spektroskopija

Abstract

In the last two decades, studies on organic molecules mimicking substances of fundamental importance in nature, like chlorophyll or hemoglobin, have attracted researchers' attention. These molecules are building blocks for a family of materials also referred to as "organic semiconductors". Such compounds can be implemented in numerous applications, ranging from data-storage to light harvesting. Some of their fundamental advantages include low cost, light weight, relatively easy engineering and mechanical flexibility, compatible with bending plastic substrates.

In this thesis work we investigated the chemical, structural and electronic properties of cobalt phthalocyanines (CoPc). These molecules have promising applications in the field of magnetic data storage and spintronics in general, due to the ferromagnetic properties of the cobalt atom. Several techniques like photoemission core-level spectroscopy and valence band spectroscopy, together with X-ray absorption, have been used in order to determine the CoPc properties in gaseous phase, i.e. in the absence of interaction with the surrounding environment.

Another set of experiments was devoted to the commissioning of the CITIUS time-resolved photoemission setup, that will be used in future studies of CoPc molecules on surfaces.

Key words: Cobalt phthalocyanine (CoPc), photoemission spectroscopy (PES), X-ray absorption spectroscopy (XAS), synchrotron radiation, laser, high order harmonic generation (HHG), time resolved spectroscopy

Table of contents

1 Introduction

Materials science is an interdisciplinary research field with potential tremendous impact on future technology. It includes physics, chemistry and engineering, and it deals with the discovery, design and engineering of new materials that may have applications ranging from catalysis to light harvesting or energy storage, and from data storage to medical products, just to mention few examples.

In recent years, scientists' attention has been attracted by organic molecules mimicking those substances of fundamental importance in nature, like chlorophyll or hemoglobin. So a new family of materials, named "organic semiconductors", OSCs, found applications in Organic Light-Emitting Diodes (OLEDs), Organic Photovoltaic (OPV), and in new fields such as electric memories for non-volatile data storage [1] and Organic Field Effect Transistors (OFETs). Generally, OSCs offer many fundamental advantages, including low cost, lightweight, large area coverage, relatively easy engineering of molecular properties and mechanical flexibility compatible with plastic substrates. Interesting opportunities for OSCs have recently emerged in the field of spintronics [2].

This latter field has interesting industrial applications for a new generation of hard disks, with reduced dimensions and costs. Since the discovery of the Giant Magneto-Resistance (GMR, [3]) in 1988, storage density increased rapidly and allowed for the realization of high capacity hard disks with smaller dimensions and cheaper production costs. In recent years devices based on Tunneling Magneto-Resistance (TMR) [4] have actually beaten the GMR devices, but they have also shown problems with the downsizing, that is making them unstable at high frequencies.

A promising idea for the downsizing of magneto-resistance based devices is to apply GMR building blocks on single molecules. To reach this objective it is necessary to characterize the chemical, electronic, and structural properties of a new family of organic molecules, the so-called molecular magnets. Typically they consist of a magnetic ion, surrounded by an organic ligand. The ion carries a spin, and serves as

magnetic bit, whereas the organic ligand has the double purpose of stabilizing the spin of the ion and shielding it from external influences. Phthalocyanines hosting a transition metal in their molecular ligand centre are promising systems for applications as magnetic bits.

For the final implementation into working assemblies, these molecules have to be placed on a surface. But since the interaction with the substrate can alter their intrinsic electronic properties, their initial characterization shall be performed in the gas phase, i.e. with no interactions.

The work presented in this thesis is part of a larger collaboration project among the University of Uppsala in Sweden, the C.N.R.-I.O.M laboratory of Trieste and the University of Nova Gorica. Aim of the collaboration is to study these new materials, from the elementary and isolated building blocks to the complex implementation in a device structure, exploiting the expertise of the whole partnership, that includes spectroscopic characterization techniques as Photo Electron Spectroscopy (PES), Inverse Photoemission (IPES), X-ray Absorption Spectroscopy (XAS) and Resonant Photo Emission Spectroscopy (ResPES) as well as time-resolved spectroscopy based on High Harmonics Generation (HHG) light sources.

In the following, we will present spectroscopic characterization of the cobalt phthalocyanine and the commissioning of the experimental set up for time resolved photoemission experiments. In Chapter 2, we will introduce the family of organic molecules of porphyrins and phthalocyanines. In Chapter 3 all the experimental techniques like core level photoemission spectroscopy (XPS), valence band photoemission, and X-ray Absorption Spectroscopy (XAS), used for data acquisition, will be described.

Chapter 4 will describe the experimental set up of the beam line and of the end station of the Gas Phase beam line of Elettra [5], where the experiments on the single molecules have been performed, while in Chapter 5 the measured gas phase data will be reported and discussed.

Finally, in Chapter 6, the commissioning of the time resolved photoemission apparatus at the “Laboratory of Quantum Optics” (LKO), of the University of Nova Gorica, will be presented.

2 Organic molecules: porphyrins and phthalocyanines

Discovered in the beginning of the 19th century, phthalocyanines immediately proved to be special kind of molecules, due to their extreme resilience and vivid colors [6]. In the beginning phthalocyanines (Pc) were primarily used as dyes, particularly blue and green. Later they have been used for their catalytic properties, and have been thoroughly studied for this application [7]. The structure of phthalocyanines is closely related to that of most important organic molecules in nature called porphyrins (Fig. 2.1, (a)). Examples of such molecules are hemoglobin (b) and chlorophyll (c). This characteristic made phthalocyanines (Pc) interesting as one of the building blocks of "organic nanotechnology", the new field of research that aims at bringing nature-like organic systems, efficiently used by living organisms and turning them into efficient "tools" in man-made devices. These molecules are expected to find use as optical materials, sensors, organic semiconductors, etc.

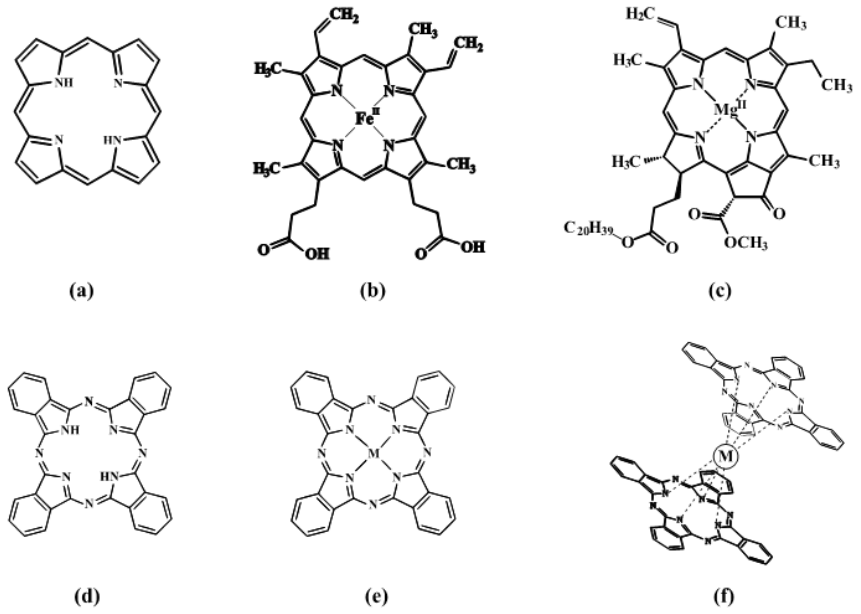

Figure 2.1. Molecular structure of: (a) metal free porphyrin, (b) hemoglobin, (c) chlorophyll, (d) Metal-free phthalocyanine, (e) Metal-phthalocyanine, (f) Double decker metal-phthalocyanine [8].

The main structure of the molecule is composed of four pyrrole rings connected by nitrogen atoms. There are three forms of widely studied phthalocyanines: the metal-free phthalocyanine also noted as H_2Pc (Fig. 2.1 (d)), where two opposite nitrogen atoms are connected to two hydrogen atoms forming a molecule with two fold symmetry, whose complete chemical formula of Pc is $H_2C_{32}N_8H_{16}$.

Other interesting forms of Pcs are the metal-phthalocyanines (e) or MPc ($MeC_{32}N_8H_{16}$) these molecules have a transition metal embedded in the central position. Among the most studied MPc's are the FePc (iron), CoPc (cobalt), NiPc (cickel) CuPc (copper). In general MPc's show great promise for application to electronic devices from photovoltaics [9], spintronics [2], semiconductors [10] etc.

The third form of phthalocyanines is called double-decker phthalocyanines, MPc_2 (f). These are formed by two phthalocyanine molecules connected by the central metal atom. These molecules are very reactive to gas molecules making them particularly interesting as gas sensors or catalysts.

The focus of this thesis work is on metal-phthalocyanines with a central metal atom exhibiting ferromagnetic properties. Their chemical and thermal resilience allows one to embed them in many systems, while their low vapor pressure in the range of 10^{-14} mBar allows to study them in UHV (Ultra High Vacuum) conditions.

The model system of a device based on phthalocyanines, consists of films of molecules deposited on different substrates [11, 12, 13], that can vary from graphite to silicon, gold, etc, in the single crystal form. The choice of the substrate varies with the molecular properties we are interested in.

3 Experimental techniques

3.1 Photoemission spectroscopy

Photoemission spectroscopy has been established as one of the most important methods to study the electronic structure of molecules, solids and surfaces. It uses photons as a probe to extract electrons from the material under investigation, as sketched in Fig. 3.1(a). If the energy distribution of the emitted electrons is plotted as in Fig. 3.1(b), their number per energy interval (I(E)) is proportional to the density of states (N(E)) inside the sample. This is an attractive feature of PES: it is able to provide information on the electron energy distribution in a material.

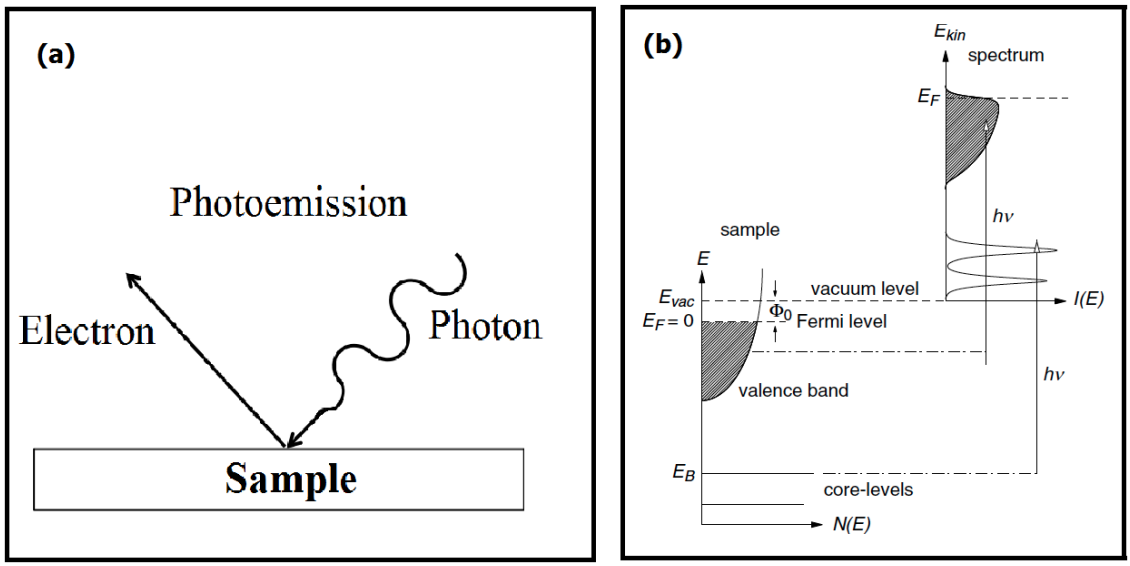

Figure 3.1, (a) basic scheme of a photoemission process, (b) Relation between the energy levels in a solid (bottom) and the electron energy distribution produced by photons of energy $h\nu$ [14].

In Fig. 3.1 (a), is shown a schematic view of a single electron photoemission from solid sample. While Fig. 3.1 (b) shows how the electronic structure of the sample manifests itself in the spectrum. A core level electron can be emitted if the photon energy is larger than its binding energy plus the work function of the sample $(E_B+\Phi_0)$. The electrons emitted from valence band have a high kinetic energy E_{kin},

compared to core-levels, due to the fact that their binding energy is relatively close to vacuum level E_{vac}.

The general idea about photoemission is expressed by the energy conservation rule [15] during the process of single electron emission. The energy of the system before electron emission can be written as the energy of a system of *N* electrons, $E_i(N)$, plus the energy of the impinging photon *hv*, while the energy after electron emission can be written as the final energy of system containing *N-1* electrons, $E_f(N-1)$, plus the kinetic energy of the emitted electron, E_{kin}. The balance equation reads:

$$E_i(N) + h\nu = E_f(N-1, k) + E_{kin}. \tag{3.1}$$

Knowing that the binding energy $E_b(k)$ is given by the difference between the final and the initial state $E_b(k) = E_f(N-1) - E_i(N)$, one can write the well known relation between the kinetic and binding energies of electrons:

$$E_{kin} = h\nu - E_b. \tag{3.2}$$

However the equation (3.2) is not taking in consideration the fact that the photoemitted electron needs to overcome the potential of the solid. Thus the relation for real photoemission experiments looks like:

$$E_{kin} = h\nu - E_b - e\phi_0, \tag{3.3}$$

where ϕ_0 is the work function of the sample.

The simplest way to estimate the binding energy of an electron is based on the Koopman's theorem [15] also known as frozen orbital approximation. In this theorem the photo excited electron is treated separately and the rest of the system is assumed to be unperturbed by the process. By applying Koopmans's theorem, one can identify the binding energy (E_b) with the negative orbital energy (ε) of the photoemitted electron: $E_b = -\varepsilon$ (Fig. 3.2, (b)). But Koopman's theorem does not account for the residual *N-1* electrons that may relax and reorganize in order to minimize their energy.

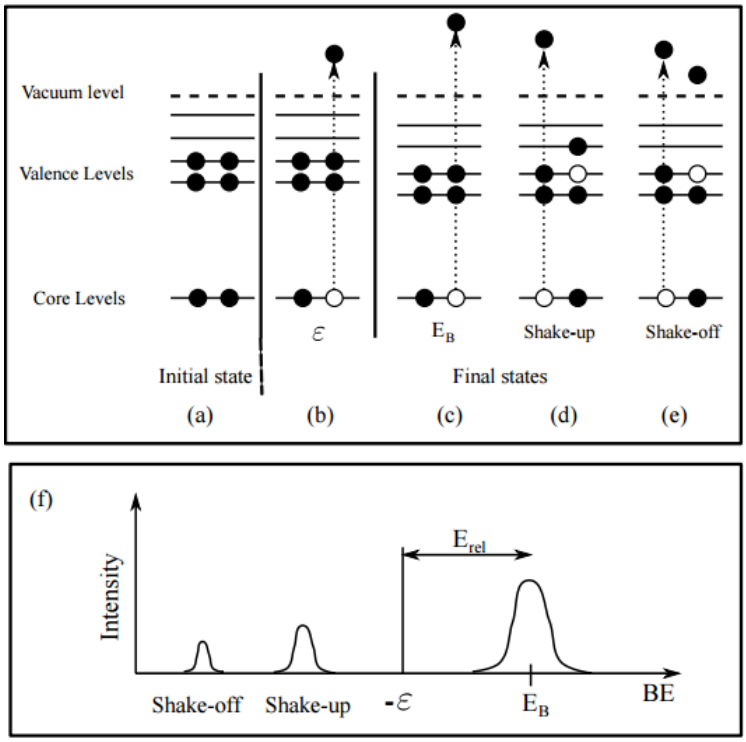

Figure 3.2, schematic view of deviations from Koopmans theorem, the electronic view (top) and the resulting spectrum (bottom) [8].

The presence of a core hole in the photoemission process can lead to the relaxation of the residual energy. In the simplest case this residual energy is transferred to the kinetic energy of the photoemitted electron and the binding energy in the spectrum gets shifted by the energy it gains due to the relaxation, E_{rel} (Fig. 3.2, (c)). In other cases the residual energy is transferred to valence band electrons that can be excited to a higher unoccupied (Fig. 3.2, (d)) or continuum (Fig. 3.2, (e)) states, giving rise to the so called "shake-up" and "shake-off" satellite peaks in the spectrum.

Again, as we can always treat an event of an electron emission from an atom as a transition of a system of *N* electrons into a system of *N-1* electrons, we have a system that undergoes a transition from initial state of *N* electrons, described by a wave function ψ_i to a final state of *N-1* electrons with the wave function $\psi_{k,s}$, where the parameter *k* stands for the momentum of the photoemitted electron and the index *s* refers to the collection of other quantum numbers identifying the final state.

The intensity of the photoemission peaks is given by the probability of the transition between the initial and final states ($\psi_i \rightarrow \psi_{k,s}$). Such a probability is in turn given by Fermi's golden rule [16]. Assuming a perturbation Hamiltonian H, the probability of transition per unit time between the two states ψ_i and $\psi_{k,s}$, is proportional to:

$$\sum_s \left|\langle \psi_{k,s} | H | \psi_i \rangle\right|^2 \delta(E_f - E_i - h\nu). \tag{3.4}$$

Where E_i and E_f are the energies of the initial and final states, δ represents the Dirac delta function.

Typically we distinguish the weakly bonded valence electrons and the strongly bonded core level electrons. The technique focusing on the core level electrons is called Core level photoemission or X-ray Photoelectron Spectroscopy (XPS), due to the fact that photons in the range of X-rays and soft X-rays are necessary to extract these electrons from their atoms. In the case of gas phase experiments the spectrum of a core level electronic state consists of sharp peaks due to the well-defined orbital energies of core levels. Thus the peak width is defined by the overall apparatus resolution and the lifetime of the created electron hole.

Despite the fact that core level electrons do not take part in chemical bonds, their binding energy is still sensitive to their chemical environment, thus different chemical environments may lead to different binding energies. The displacement of binding energy is called "chemical shift" and is due to alteration of electronic potential in the valence band where electrons can participate in chemical bonds with other atoms. When multiple atoms of the same atomic species have different chemical environments, as in the case carbon and nitrogen in phthalocyanines, multiple peaks with different chemical shifts can appear. Based on this, it is possible to extract valuable information on the structural properties of the molecule, as it will be seen in Chapter 5.

Valence electrons belong to the outermost electronic levels; these levels take part in the interactions with neighboring atoms. Valence electrons may also form hybridized orbitals, during the process of bonding between atoms. The involved orbitals morph and create a mixed orbital exhibiting properties of both orbitals involved in the

process. Due to ionization cross section of valence electrons, valence PES requires photons in the range of UV and XUV *(5-150) eV* in order to achieve electron emission; for this reason it is also named Ultraviolet Photoelectron Spectroscopy (UPS).

3.1.1 Auger process

Whenever an atom is illuminated by a highly energetic photon (Fig. 3.3. step 1.) capable of extracting an inner shell electron, a core shell electronic vacancy is created. This vacancy is either filled by an electron from a more energetic shell (a shell closer to the vacuum level) or an electron from valence band. As this electron "falls" into the inner shell it releases energy, in an amount that equals the energy difference of the two energy levels involved in the process. In the example presented in Fig. 3.3, it is the energy difference between L_1 subshell and K shell.

The residual energy can generate two events:

i) The emission of a photon with the energy $E_{photon}=E_{L1}-E_K$,

ii) The emission of an electron from the same shell that was occupied by the electron that filled the core hole. In the case presented in Fig. 3.3 it is an emission from $L_{2,3}$ level. This kind of electron has been named "Auger electron". The kinetic energy of this electron is equal to $E_{Auger}= E_{L-K}-E_{bind\ L2,3}$.

Where the E_{L-K} is the energy released in step 2. and $E_{bind\ L2,3}$ is the binding energy of the electron in step 3. of Fig. 3.3.

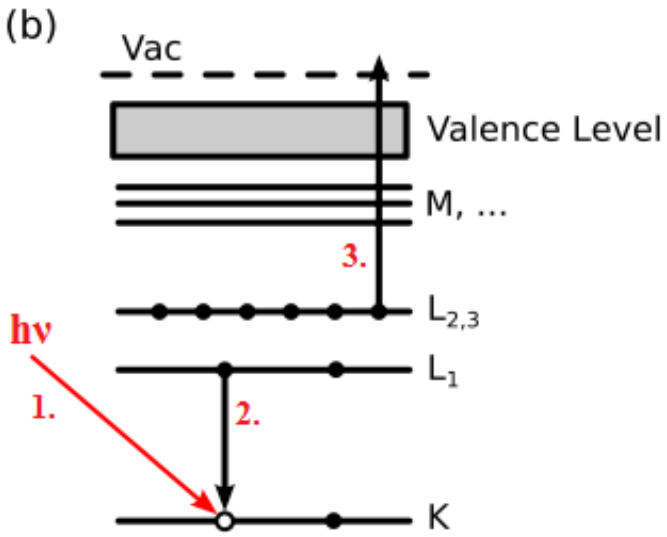

Figure 3.3, an example of the three steps of the Auger process: 1.) Creation of core hole in an inner shell, 2.) Filling up of the inner shell from a higher shell 3.) Emission of an Auger electron from the higher sub-shell [17]

The notation for the Auger transition is based on the sequence of involved shells and sub shells. The case of Fig. 3.3 shows a $KL_1L_{2,3}$ Auger transition. In this thesis we will also refer to LVV Auger transitions, where the V stands for the valence band.

Auger electrons are particularly interesting for calibration purposes of gas phase measurements, since their kinetic energy is always the same independently from the photon energy used to create the core-hole.

3.2 X-ray Absorption Spectroscopy (XAS)

Like photoemission spectroscopy, XAS is also driven by the same process of electronic excitation. The probability of a photon being absorbed can be expressed by the Fermi golden rule:

$$\omega \propto \left|\langle \psi_f | \boldsymbol{e} \cdot \boldsymbol{p} | \psi_i \rangle\right|^2 \rho_f(E) \tag{3.7}$$

Where $\boldsymbol{e}$ is the polarization unit vector and $\boldsymbol{p}$ is the linear momentum operator, while $\rho_f(E)$ is the density of unoccupied states. In XAS process the core level electrons are excited into unoccupied valence band levels. The relaxation can occur as fluorescent decay leading to an emission of a photon or as an Auger decay leading to the emission of an Auger electron.

In this technique the photon energy is scanned over an absorption edge of a core level. For a given absorbing element, the general decrease in X-ray absorption coefficient with increasing energy of incident photon is interrupted by a sharp rise when the energy is equal to the binding energy of an electron shell (K, L, M, etc.) in the absorber; this energy is the minimum energy at which a vacancy can be created in the particular shell and is referred to as the "edge".

Absorption can be measured in two different ways, looking at transmission or at electron yield. In transmission the intensity of the light is monitored before and after the sample using ionization cells, the ratio between the two intensities being related to the absorption coefficient. When measuring the electron yield, as we did in our experiment (described in Chapter 4), different setups can be used:

- total electron yield, i.e. all electrons emitted during the process are measured;
- partial electron yield, a retardation voltage in front of the detector is used to block low energy electrons;
- Auger electron yield, the retarding voltage is set to select only electrons from the selected Auger transitions.

In general, X-ray absorption spectroscopy is a challenging technique that requires a stable high resolution X-ray source tunable in a wide energy range and a sensitive detection system. This is why the technique is used exclusively in combination with synchrotron based light sources. In our experiment, we made use of a particular type of XAS, i.e. Near Edge X-ray Absorption Fine Structure (NEXAFS).

NEXAFS is a particularly efficient tool for probing directional bonds, as the ones present in organic molecules, as benzene, pyrrole, phthalocyanine, etc. The electric field vector of the linearly polarized light can be used as a probe in order to look for bonds of the same orientation. In this way it is possible to determine the orientation of molecules absorbed on surfaces. For the particular case of NEXAFS in gas phase, the random orientation of molecules evaporated in vacuum results in an overlap of signal from in plane and out of plane molecular orbitals [18].

4 Experimental setup

4.1 Gas phase beam line

The gas phase experiments were carried out at Elettra Synchrotron radiation facility, which is a 3rd generation synchrotron radiation source located in Basovizza, Trieste (Italy). The Elettra storage ring uses 2.0 GeV or 2.4 GeV electrons in order to emit photons in the range from few eV to several keV. Since 2010 Elettra's storage ring is equipped with a booster (a smaller electron accelerator with ring structure), which makes possible to operate in the so called top up mode. In top up mode electron bunches are continuously injected into the storage ring, in order to compensate for the losses due to synchrotron emission, thus allowing to work with a constant flux of photons. In this way a stable beam is produced and maintained for several days in a row, and stable and reproducible measurements can be performed.

Gas Phase beam line [19] is a high resolution beam line devoted to the studies of gaseous systems at pressures up to 10^{-4}mBar. The covered energy range varies between 13 eV and 900 eV, with an optimal resolving power (i.e. $E/\Delta E$) varying between 10000 and 28000, depending on the working energy. The beamline uses three tunable undulators whose gap can be tuned to optimize the photon flux at the desired photon energy.

The schematic view of the beam line is shown in Fig. 4.1. It contains the prefocusing mirror, a variable angle spherical grating monochromator, where the spherical grating allows for the use of a fixed exit slit, which finally determines the resolution of the photon beam.

The monochromator is equipped with six different gratings to select the appropriate photon energy, resolution and flux. The photon flux at this beam line is decreasing with the increase of photon energy (see Table 4.1).

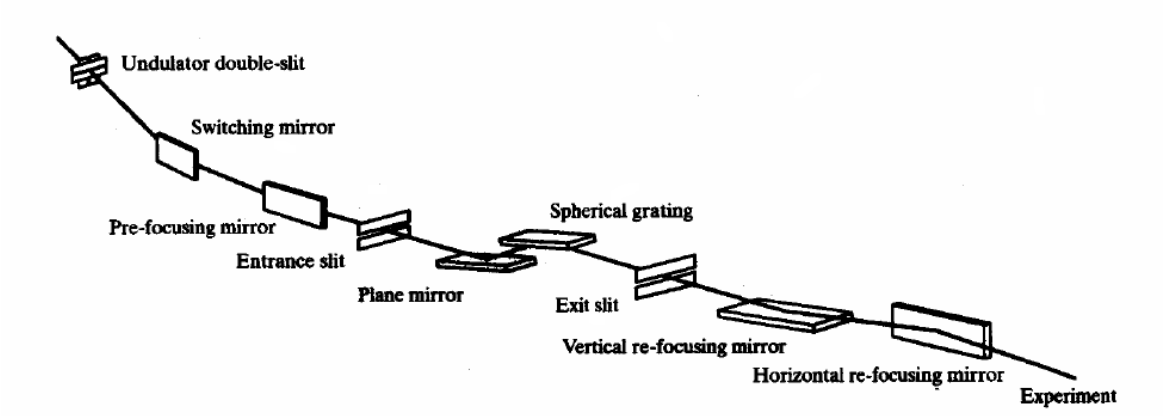

Figure 4.1. Schematic view of the optical setup in tha Gas Phase beam line, [20].

Two refocusing mirrors allow for an almost circular spot at sample position with the size of 200 μm by 200 μm. To perform the XAS experiments, the monochromator can be used in a high resolution scanning mode, where the first mirror (Plane mirror on Fig 4.1) is held fixed and only the spherical grating, selected accordingly to the desired energy range is being moved.

Table 4.1, Specifications of the gratings of the Gas phase beam line monochromator, energy range, flux and best resolution.

Grating	Energy range (eV)	Max resolving power $(E/\Delta E)$	Flux (ph/sec/100mA)@selected
G1	13-60	25 000	6.3e10 @ 45eV
G1 2nd order	40-90	28 000	2.2e11@ 65eV
G3	80-180	10 000	1.5e11@ 86eV
G4	160-430	12 000	1.5e10@ 245eV 1.1e10@ 401eV
G5	360-900	10 000	2.0e10@ 540eV 3.0e9@ 680eV
G6	13-25	10 000	5.0e11@ 20eV

4.2 End Station

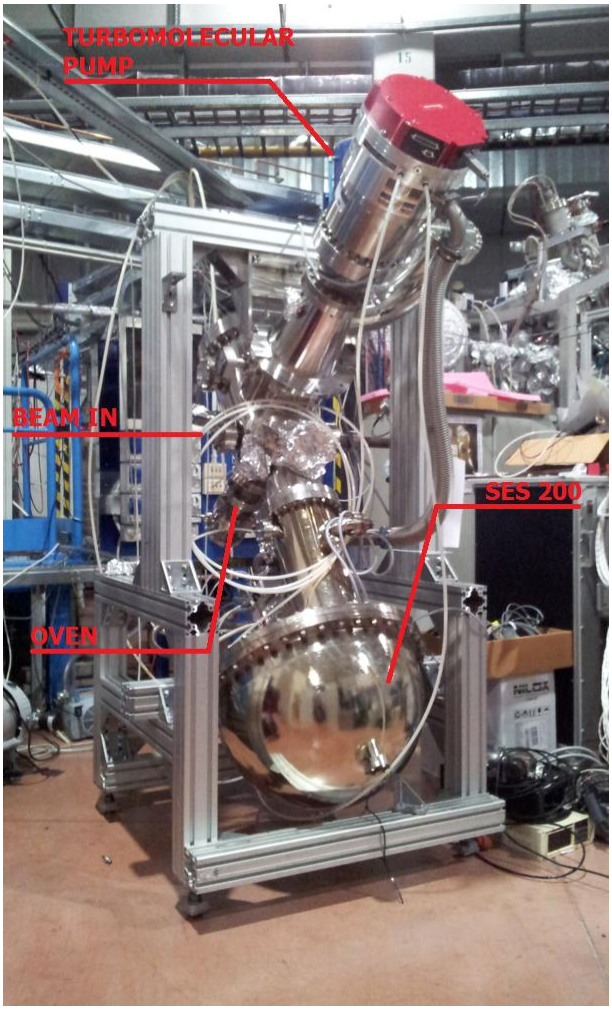

Figure 4.2, Image of ULLA end station a SES200 analyzer (bottom), a large turbomolecular pump (top) and a frame that allows the analyzer to be mounted under the magic angle with respect to the field of the incoming light.

Gas phase beam line can host different end stations. For our experiment we used a high energy resolution photoemission chamber, named ULLA (ULtrafast Laser Assisted spectroscopy), since it was originally assembled within the collaboration of Uppsala University and the Gas Phase beam line to perform time-resolved photoemission experiments, during the commissioning of the CITIUS light source [21, 52].

ULLA is equipped with a SES-200 hemispherical electron analyzer [22] from VG-Scienta Ltd. The chamber frame was specifically designed to set the lenses axis of the analyzer at the magic angle (i.e. 54.7 degrees) with respect to the electric vector of the incident synchrotron light. At this angle the asymmetry contributions to photoelectron current are minimized [23]. Standard gas phase experiments do not require ultra high vacuum. However in such experiments the sample molecules are constantly flowing in the chamber, which can pose quite a challenge to maintain high vacuum conditions. Thus a vacuum chamber devoted to gas phase investigations must be equipped with an efficient pumping system. Additionally, removal of water from the vacuum surface is eventually needed in order to avoid vacuum contamination when running experiments at very low vapour pressure, or in case of metastable and highly reactive molecules. In our experiments the end-station was pumped by a 1600 l/s magnetically levitated turbomolecular pump. To improve vacuum, a copper trap was cooled by liquid nitrogen (see sample stage, Section 4.3). The trap was crucial also to prevent the deposition of the molecule inside the chamber and to reduce water contamination of vacuum.

4.2.1 Hemispherical electron spectrometer

An hemispherical electrons' spectrometer, also referred to as concentric hemispherical spectrometer, is an instrument to measure the kinetic energy and the emission angle of photoemitted electrons. A modern hemispherical spectrometer, as the one sketched in Fig. 4.3, consists of a set of electrostatic lenses that transport electrons to the entrance slit, and two hemispheres, that are filtering the electrons in energy. The lenses are designed to define the analyzed sample area, the maximum angular acceptance of photoemitted electrons, and to accelerate or decelerate the particles.

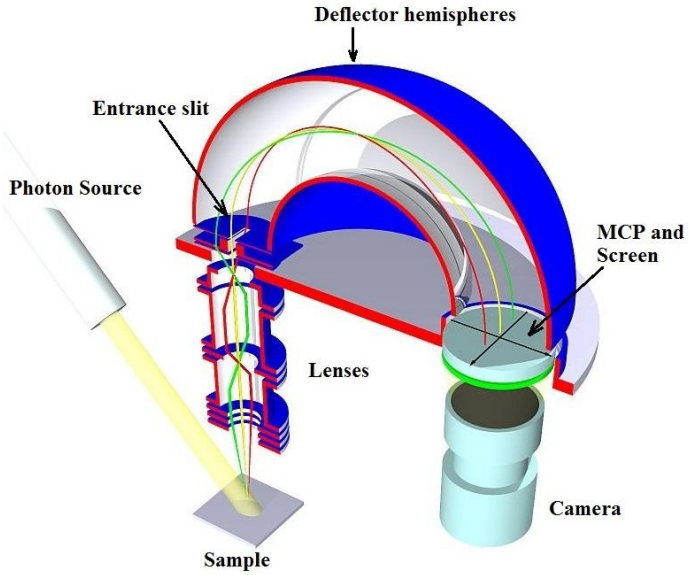

Figure 4.3 Cross-sectional view of an operating hemispherical analyzer. The colored lines represent the electron's trajectories [24]

The entrance slit aperture affects the resolution of the analyzer. A narrower slit aperture can improve the resolution of the analyzer, however at the expense of the electron transmission. Before electrons enter the spherical deflector a retardation potential is applied. This potential is used to decelerate electrons in order to improve the resolving power of the kinetic energy. Intrinsically a better resolving power can be achieved when slower electrons enter the hemispheres; on the other hand slowing down the electrons allows for transmission of a smaller kinetic energy window through the spheres. The deflector guides the electrons through its electric field making the slower (less energetic) electrons deflect more than the fast (more energetic ones). At the end of the deflector the transverse position of the electron on the screen gives us the information about its energy while the longitudinal position provides information about the original angle of emission.

Those particles, which enter the hemispheres normal to the entrance slit, move through the hemispheres on the central trajectory, have the nominal pass energy E_p:

$$E_p=(-q)k\Delta V \tag{4.1}$$

Where q is the charge of the particle, ΔV is the potential difference V_{out} - V_{in} applied to the hemispheres, k is a calibration constant. These particles reach the detector at the nominal radial position R_0 (average radius of the two hemispheres). If S is the dimension of the entrance slit and the spectrometer accepts the half angle α in the dispersion direction, the resolution or FWHM (full width at half maximum) of the transmitted line, ΔE_{an}, is given by:

$$\Delta E_{an}/E_p = S/2R_0 + \alpha^2/4 \qquad (4.2)$$

From eq. (4.2) it is clear that the entrance slit aperture affects the resolution of the analyzer; a narrower slit aperture can improve the resolution of the analyzer, however at the expense of the count rate.

An important parameter for electrons spectrometers is the transmission, i.e. the ratio between the electrons entering the analyzer and electrons reaching the detector. A proper set up needs to achieve the maximum transmission possible and keep it constant for all electrons with different kinetic energies. The SES200 used in our experiments had been previously characterized to check its transmission/collection efficiency and resolution performances. Tests were carried out using different combinations of pass energies and analyzer slit widths using the Ar 3p and 2p photoelectron lines as test cases. An energy resolution of about 6 meV was achieved with the 5 eV pass energy. At the same time, the energy resolution decreased with pass energy and slit openings, as expected. The analyzer was found to operate at low kinetic energies down to 1.5 eV and to have a reasonably smooth transmission function in the kinetic energy range of 8-35 eV [23].

4.2.2 XAS acquisition setup

X-ray absorption spectra can be measured indirectly by detecting the secondary processes (electron or photon emission) following the primary absorption process. We used the multichannel plate detector of the SES200 analyzer in the partial

electron yield (PEY) mode (described in Section 3.2), to be sensitive to electrons coming from a specific Auger transition (see Section 3.1.1). The lenses were set to transmit as many electrons as possible, the analyzer slits were completely opened and the pass energy was set to the maximum value of 500 eV. All of this makes the analyzer work as a funnel, allowing most of the electrons to reach the detector and contribute to the XAS signal. In order to be sensitive only to a particular transition, an energy window centered at the kinetic energy of the specific Auger transition was set. Simultaneously, a reference signal, I_0, is recorded with a photodiode placed after the interaction region, to measures the intensity of the incident photon flux. I_0 was used to normalize the XAS signal.

4.3 Sample stage

Since our interest was to study pure non interacting CoPc molecule in gaseous phase, the molecules needed to be sublimated and evaporated in a particular way in order to create a dense molecular beam in the desired position, that is at the same time the focus of the gas phase beam line optics and the centre of the analyzer field of view.

This was done by inserting the powder into a crucible, which was later inserted in an oven inside the experimental chamber; high vacuum, in the order of low 10^{-7} mBar, was maintained in the chamber when the crucible was at room temperature.

The whole assembly is designed so that crucibles containing different samples could be easily replaced without breaking vacuum in the main chamber.

The setup was designed in order to minimize thermal contact between the heating stage (Fig. 4.4, (A)) and the rest of manipulator assembly. The heating stage is mounted on a 3-axis manipulator (Fig. 4.4, (B)). It is supported on double-sided CF40 flange (Fig. 4.4, (C)) welded to a hollow rod which can be used to insert or remove crucibles from the oven, while a gate valve separates the linear translator assembly

from the main chamber. For this purpose a suitable pumping stage can be connected to the KF40 (Fig. 4.4 (D)) of our in-house built load-lock stage.

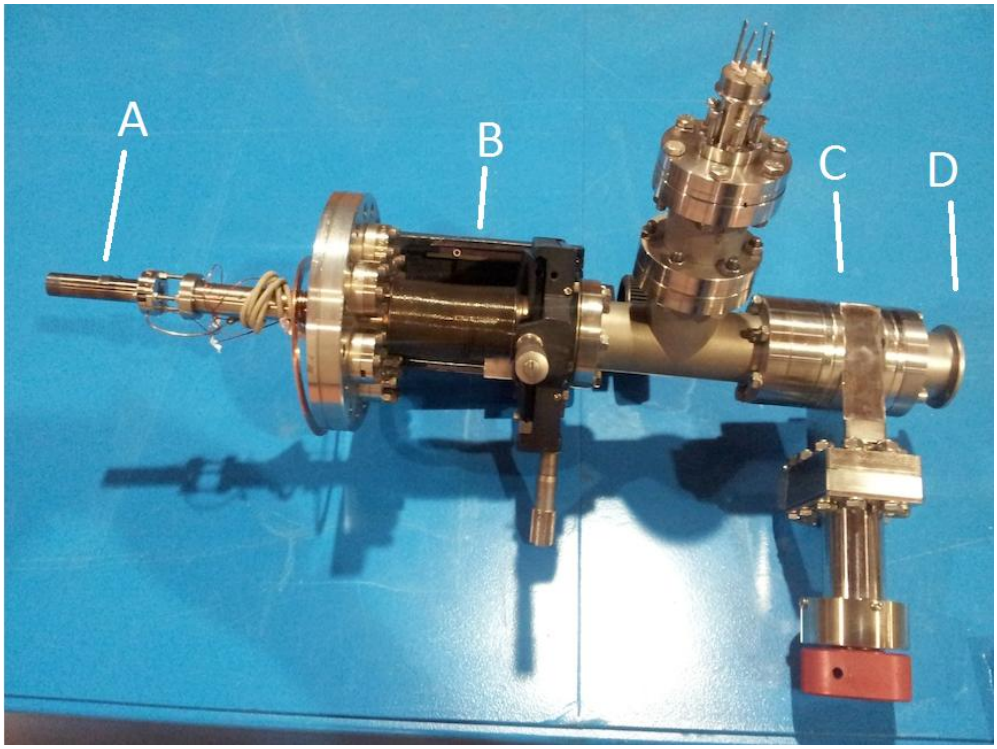

Figure 4.4, (A) the oven hosting the crucible with the sample, (B) manipulator allowing the alignment of the crucible, (C) valve, (D) flange for mounting the linear translator for sample exchange.

4.3.1 Sample preparation

The evaporation of CoPc has proven to be quite challenging. The CoPc powder even if stored in a sealed bottle, had formerly been exposed to air and air humidity. Besides those, the powder was also containing contaminants from the manufacturing process. The cleaning procedure consisted in very slow degassing at temperatures just above water desorption, monitoring residual gas analyzer spectrum. The procedure lasted for 24 hours. The temperature was then gradually increased up to 400°C to get rid of

contaminants, keeping the total pressure in the 10^{-7} mBar regime. Finally in order to obtain reasonable signal (i.e. dense enough molecular beam) from CoPc, the molecule was heated to approximately 430°C. This procedure is based on standard resistive heating however, the fact that the entire crucible could not be heated homogeneously caused condensation of CoPc on its top. The result was the formation of a "cork" at the crucible aperture, which forced us to replace the crucible few times and to repeat the cleaning procedure.

5 Experimental data

As already mentioned (see Chapter 2.), phthalocyanines are a class of stable organic or organometallic compounds. The phthalocyanine (also named metal free or H_2Pc) is a planar aromatic system (Fig. 5.1, left). The two central hydrogen atoms can be replaced by a single divalent atom, such as Mg^{2+} or a transition metal (and is generally referred to as MePc). For this thesis we selected the CoPc.

To characterize the structural properties of our sample, we acquired the XPS spectra from the different phthalocyanine elements, together with the XAS of the Co L-edge and N K-edge.

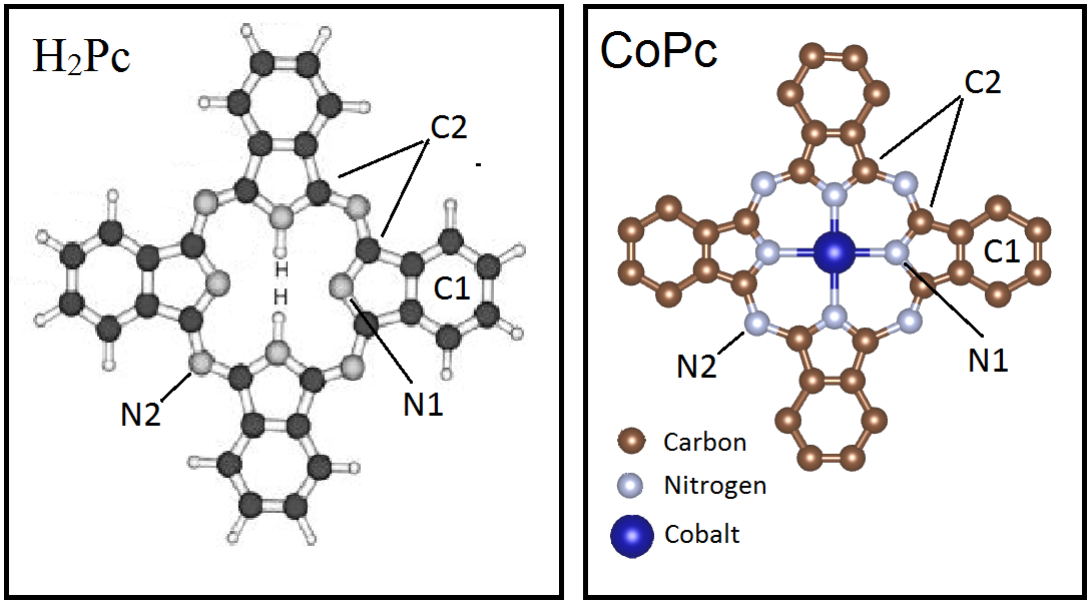

Figure 5.1, Left-structure of metal free phthalocyanine H_2Pc, Right-structure of CoPc molecule, atoms of the same atomic species in different chemical environments are labeled with N1, N2 for nitrogen C1, C2 for carbon [25].

In Fig. 5.1(right) the CoPc molecule is sketched. It is possible to distinguish immediately the different chemical environments for carbon, nitrogen and cobalt

atoms, as an example of a typical metal-phthalocyanine complex. In the case of carbon atoms, those named C1 are building up the external benzene rings, characterized only by C-C bonds; those named C2 are instead included in pyrrole rings (pentagonal), characterized by C-N bonds. In the case of nitrogen atoms N1 are included in pyrrolic rings and are also bonded to the cobalt atom, whereas N2 are the atoms connecting the pyrrole rings (bridge N atoms). Finally, the divalent cobalt atom forms a neutral complex with the Pc^{-2} ligand.

The interest of studying the CoPc is mainly related to the electronic configuration of the Co 3d shell. In the case of cobalt, the not completely filled 3d shell is responsible for its magnetic properties [26] as well as for the possible bonding of CoPc molecules to the substrate surface [27].

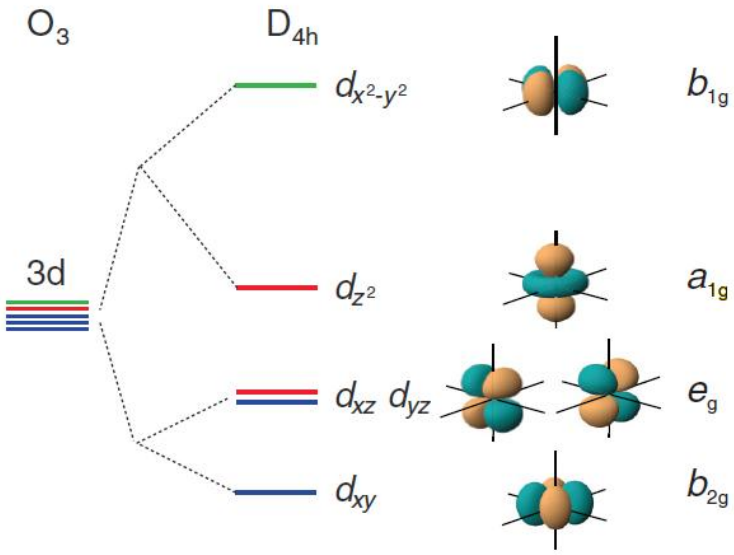

Figure 5.2. The energy splitting of the Co 3d levels from the O_3 spherical symmetry to D_{4h} square planar symmetry [26, 27].

In Fig. 5.2 is shown a representation of Co 3d orbitals splitting due the transition from O_3 symmetry of the Co to the D_{4h} group symmetry of the CoPc molecule [26]. The original degeneracy is removed generating three singlet states $3d_{xy}$ (b_{2g}), $3d_{z2}$ (a_{1g}), $3d_{x2-y2}$ (b_{1g}) and one doublet $3d_{xz}$ $3d_{yz}$ (e_g). The empty b_{1g} state is hybridized with π orbitals of the nitrogen atom, the occupied in plane state b_{2g} is also delocalized in the surrounding hybrid nitrogen bonds. The $3d_{z2}$ (a_{1g}) and the doublet $3d_{xz}$ $3d_{yz}$ (e_g)are mainly localized on the central atom [27, 28, 29, 30]. A correct assignment of the

spectral features generated by these states is fundamental to characterize the electronic properties of the molecule.

In the following Sections the experimental data will be presented and discussed. XPS from carbon, nitrogen and cobalt were measured for two reasons: to confirm the chemical and structural properties of the molecule, in the case of C 1s (Section 5.1) and N 1s (Section 5.2), and to determine the correct energy range for the absorption edges for the XAS and for the resonant photoemission measurements (the latter are not presented in this thesis) in the case N 1s and Co 3p.

The presentation of absorption spectra on the Co L-edge and N K-edge will follow. This study allowed us to map the distribution of empty states related to cobalt and nitrogen. Finally the valence band investigation as function of photon energy will be presented in order to obtain information about the precise energy positions of the occupied molecular states.

The combination of XAS and valence band measurements will provide complementary results, allowing to get the full information about the energetic structure of the D_{4h} split Co 3d states.

5.1 Carbon 1s XPS

The measured C 1s XPS spectrum of CoPc is plotted in Fig. 5.3. It has been acquired at the photon energy of 392 eV and it has been calibrated relative to the C 1s peak of the CO_2 calibration gas [31, 32]. The spectrum has a good signal to noise ratio and clearly shows three spectral features. From literature [35, 36] it is known that the C 1s spectrum of CoPc consists of four peaks. Thus our spectrum was fitted using four Voigt functions, and the fir parameters are listed in Table 5.1. Voigt shape [34] is a convolution of a Lorentzian and a Gaussian distribution function. The Gaussian profile accounts for the broadening due to the experimental resolution, while the Lorentzian broadening is due to the lifetime of the hole created by the photo emitted

electron. Effects due to different vibrational transitions, and in the case of carbon atoms in the benzene ring, also slightly different chemical environments, have not been taken into account in our deconvolution.

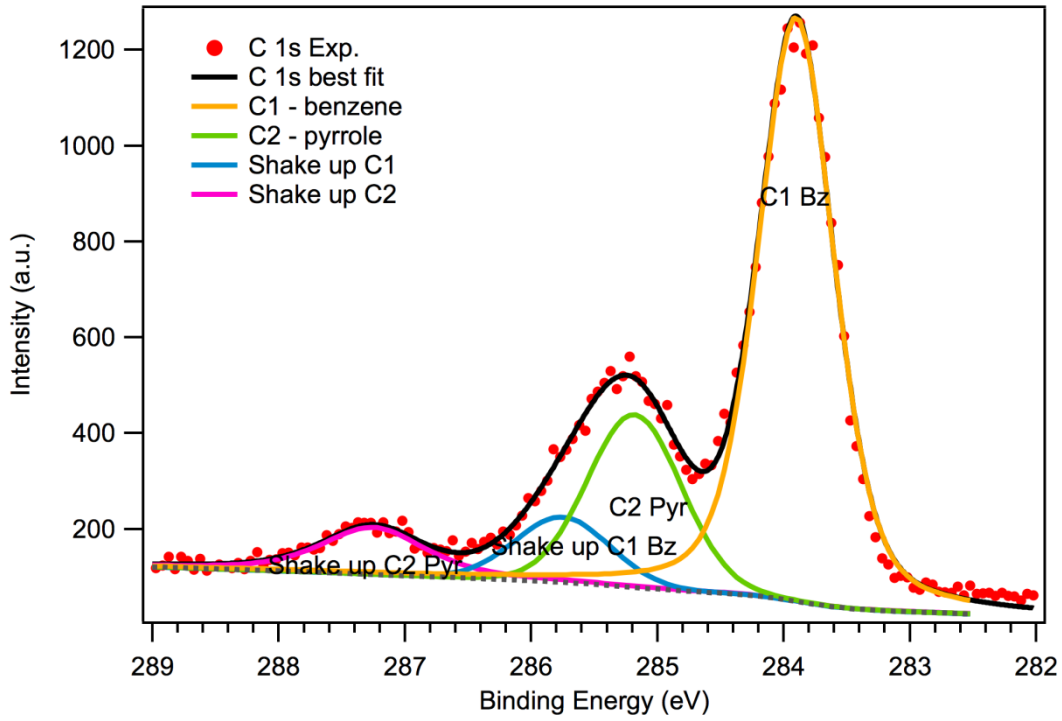

Figure 5.3, C 1s XPS spectrum of CoPc in gas phase, raw data, fit, and fitting curves of all spectral components, hν = 392 eV.

The most intense peak is assigned to carbon atoms in benzene rings (Fig. 5.3, "C1"). The second highest peak consists of two components: the most important comes from the carbon atoms of the pyrrole rings (Fig. 5.3, "C2"), while the second component is due to the shake-up transitions of the benzene carbon atoms (Shake up "C1"). Finally the third peak (Shake up “C2”) is due to shake-up transition in the carbon atoms of the pyrrole rings [33].

In total there are 32 carbon atoms in the phthalocyanine molecule, 24 of which are benzene carbon atoms while 8 of them are pyrrole carbon atoms. This ratio manifests itself in a 3:1 intensity ratio between the C1 benzene peak and C2 pyrrole peak of Fig. 5.3.

Table 5.1: Fit parameters for C 1s XPS data, i.e. binding energy of the spectral feature, FWHM of the fitting function, and intensity corresponding to the area beneath the fitting curve.

Peak	Binding Energy (eV)	FWHM (eV)	Intensity
C1 1s benzene	283.9+/- 0.01	0.71+/- 0.01	1085.40+/- 0.02
C2 1s pyrrole	285.18+/- 0.05	0.71+/- 0.05	341.81+/- 0.05
C1 benzene Shake up	285.75+/- 0.21	0.95+/- 0.25	128.92+/- 0.02
C2 pyrrole shake up	287.25+/- 0.02	0.95+/- 0.25	129.51+/- 0.02

From the analysis procedure, all the appropriate spectral features corresponding to the carbon in the CoPc are present. By comparing our fitting results with other XPS measurements, of metal and non-metal phthalocyanines measured both in gas phase and thick films [35, 36], we can conclude that the structural properties related to carbon atoms in the molecules were preserved in the process of high temperature evaporation.

5.2 Nitrogen 1s XPS

The N 1s spectrum of the CoPc acquired with 495 eV photon energy is shown in Fig. 5.4. The spectrum was calibrated using the XPS N 1s emission from pure N_2 gas (BE = 409.9 eV [37]). It is possible to recognize a main structure at BE= 403.3 eV and a small feature at BE= 404.8 eV. From literature [36, 38] the main peak can be

deconvolved in two components: one due to N1 nitrogen atoms in the pyrrole ring and the other due to N2 nitrogen atoms bridging the rings.

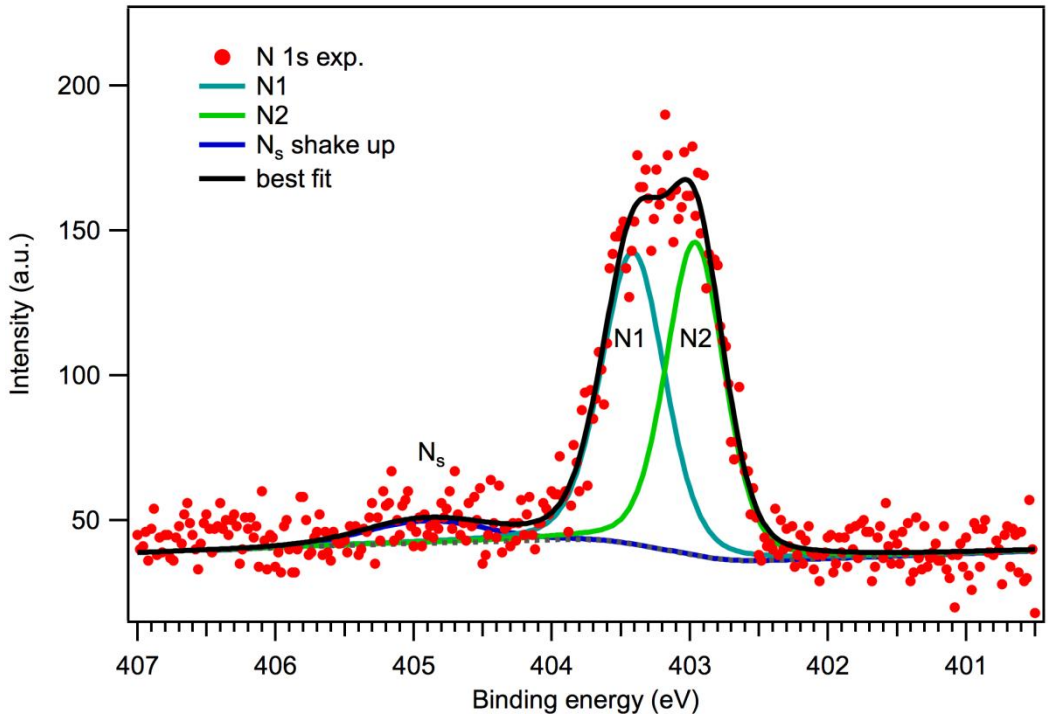

Figure 5.4, XPS spectrum of N 1s level of CoPc, with the fit and the corresponding fit components.

The data were fitted with three Voigt functions. Two functions were used to fit the main peak, to account for the two different types of nitrogen atoms, the third function was used to fit the third small peak at 404.8 eV binding energy, which comes from the N 1s shake-up transitions. Since four N atoms are connecting the pyrrole rings (see Fig. 5.1, N2) and four nitrogen atoms are placed in the centre of the molecule (Fig. 5.1, N1), an intensity ratio of approximately 1:1 characterizes the spectral components of N1 and N2 [38]. Parameters of the fit are presented in Table 5.2. Also in this case, the occurrence of possible different vibrational transitions was not taken in account.

The N 1s spectrum was found in agreement with other measurements on metal phthalocyanines [36, 38].

Table 5.2. Fit parameters for N 1s XPS data, i.e. binding energy of the spectral feature, FWHM of the fitting function, and intensity relative to the area beneath the corresponding fitting curve.

Peak	Binding Energy (eV)	FWHM (eV)	Intensity
N1 1s pyrrole	402.95+/- 0.03	0.49+/- 0.03	64.80+/- 0.05
N2 1s bridge	403.41+/- 0.03	0.55+/- 0.05	64.28+/- 0.05
N_S shake up	404.91+/- 0.13	1.02+/- 0.17	8.56+/- 0.05

5.3 Cobalt 3p XPS

At $h\nu$=120 eV, the Co 3p level was measured to determine the correct photon energy for the acquisition of the resonant photoemission spectra of the valence electrons. The spectrum displayed in Fig. 5.5 shows the 3p emission at BE=65.8 eV and a broad shoulder at BE=67.7 eV, that is difficult to interpret and could also be due to condensed flakes of CoPc molecules on the tip of the evaporation crucible.

The first feature (Fig. 5.5 (A)) is due to the Co $3p_{3/2}$ emission from molecule in gas phase, and has a binding energy 65.85 eV. The second peak, in Fig. 5.5 (B), at BE=67.52 eV, cannot instead be unambiguously assigned to the $3p_{1/2}$ spin-orbit component, since the shift is significantly higher than expected (1.7 eV, instead of 1.1-1.2 eV [58]). Nonetheless a proper energy range for the measurement of resonant photoemission data can still be extracted from the spectrum.

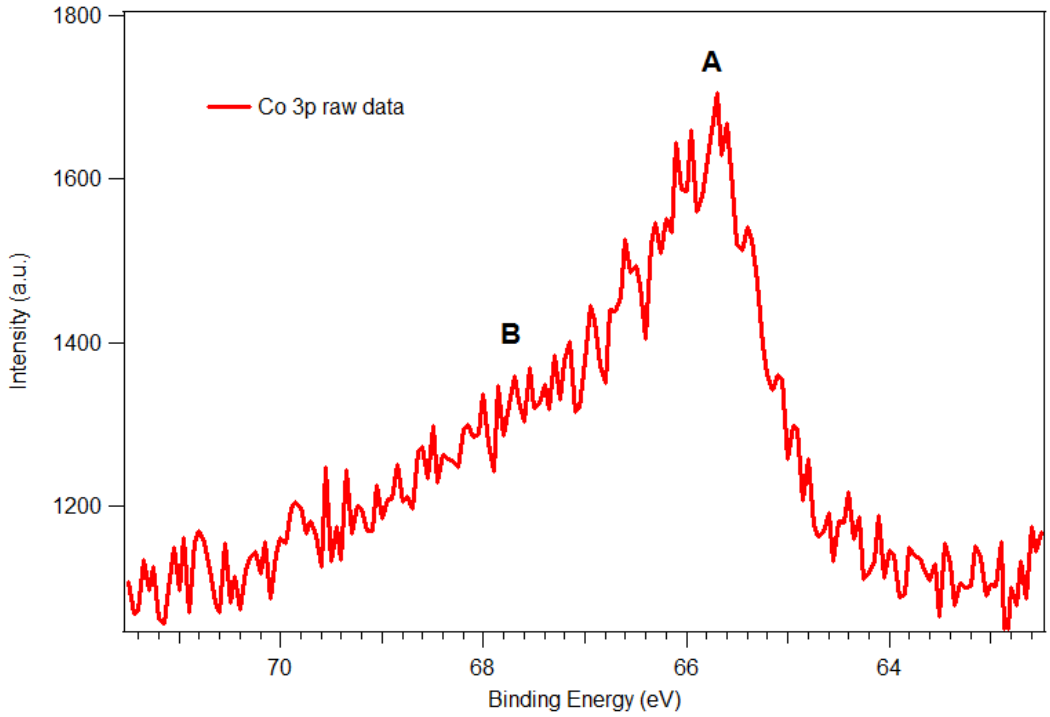

Figure 5.5: Co 3p photoemission spectrum, photon energy 120 eV.

To the best of our knowledge this is the first Co 3p photoemission spectrum in gas phase from a phthalocyanine molecule. For a complete XPS characterization of the molecule, the Co 2p XPS would have been the optimal choice, because the 3p subshell belongs to the same M shell of the 3d subshell we are interested in. However due to the very low photon flux available at the energy needed to study the 2p, it was not possible to record a spectrum of such a subshell.

5.4 Cobalt L-edge XAS

The cobalt L-edge XAS spectra shown in Fig. 5.6 were acquired using the partial yield electron detection (Section 4.2.2). Fixing the kinetic energy window of the hemispherical analyzer at a specific value, only electrons with appropriate energy are contributing to the signal. In the present case the energy window was tuned at the Auger electrons from the cobalt LMM transition. The number of detected Auger transitions is proportional to the transition probability of an electron being promoted

from a Co 2p state into a Co 3d unoccupied state. The relaxation of a valence band electron into the empty core hole can subsequently lead to the emission of an Auger electron. Due to low density of molecules, gas phase measurements of XAS are very time consuming, thus only the more intense resonance of the Co $2p_{3/2}$ was measured. For the acquisition of spectra the beam line was set to operate at high photon energy resolution, i.e., 330 meV.

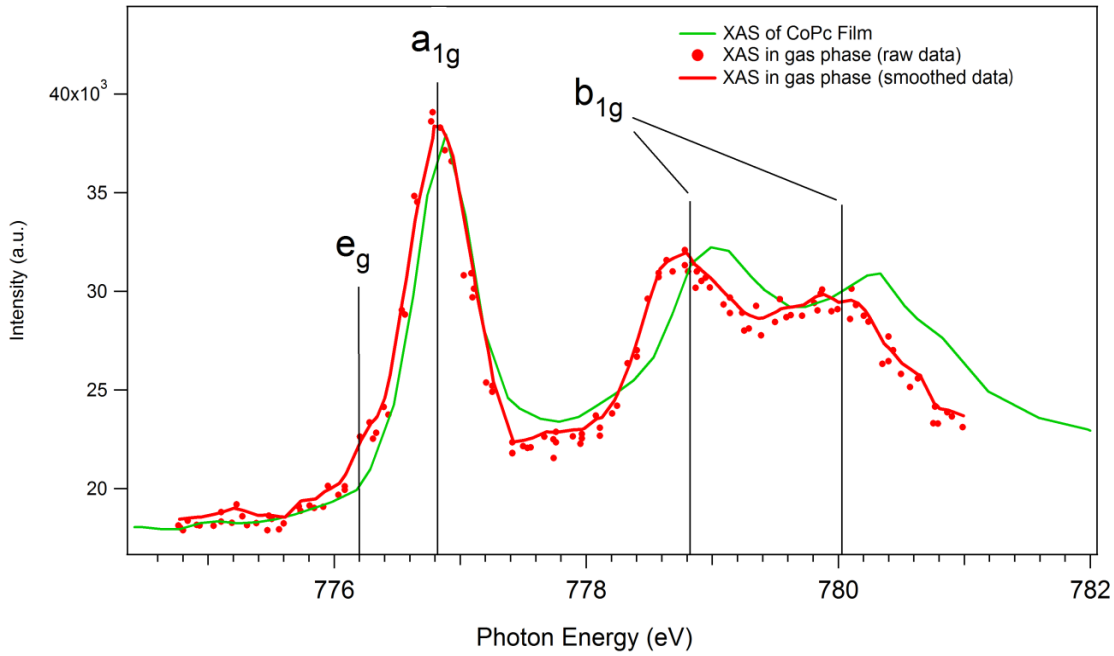

Figure 5.6, XAS spectra of CoPc $2p_{3/2}$ in gas phase, compared to spectra acquired on CoPc film (green) [28]. The green spectrum is a sum of spectra acquired at different angles between the light polarization and the surface, the separated components are shown in Fig. 5.7. Gas phase XAS raw data are represented by red dots, while the red curve corresponds to smoothed raw data. Photon energy resolution: 330 meV.

In Fig. 5.6 a gas phase measurement (red) of the CoPc L_3 edge is shown together with the L_3 edge from a molecular film grown on a Au(110) surface. From single molecule density functional theory (DFT) calculations [29, 30], it is known that the unoccupied molecular states of cobalt are the e_g level of the doublet state, the spin down component of the singlet state a_{1g} and both spin up and down components of the empty b_{1g} orbital (Fig. 5.2). Thus we can attempt to attribute the spectral features in the spectrum shown in Fig. 5.6 to their respective unoccupied electronic levels, by using as comparison, the correspondence between the theoretical calculations and XAS measurements on CoPc film.

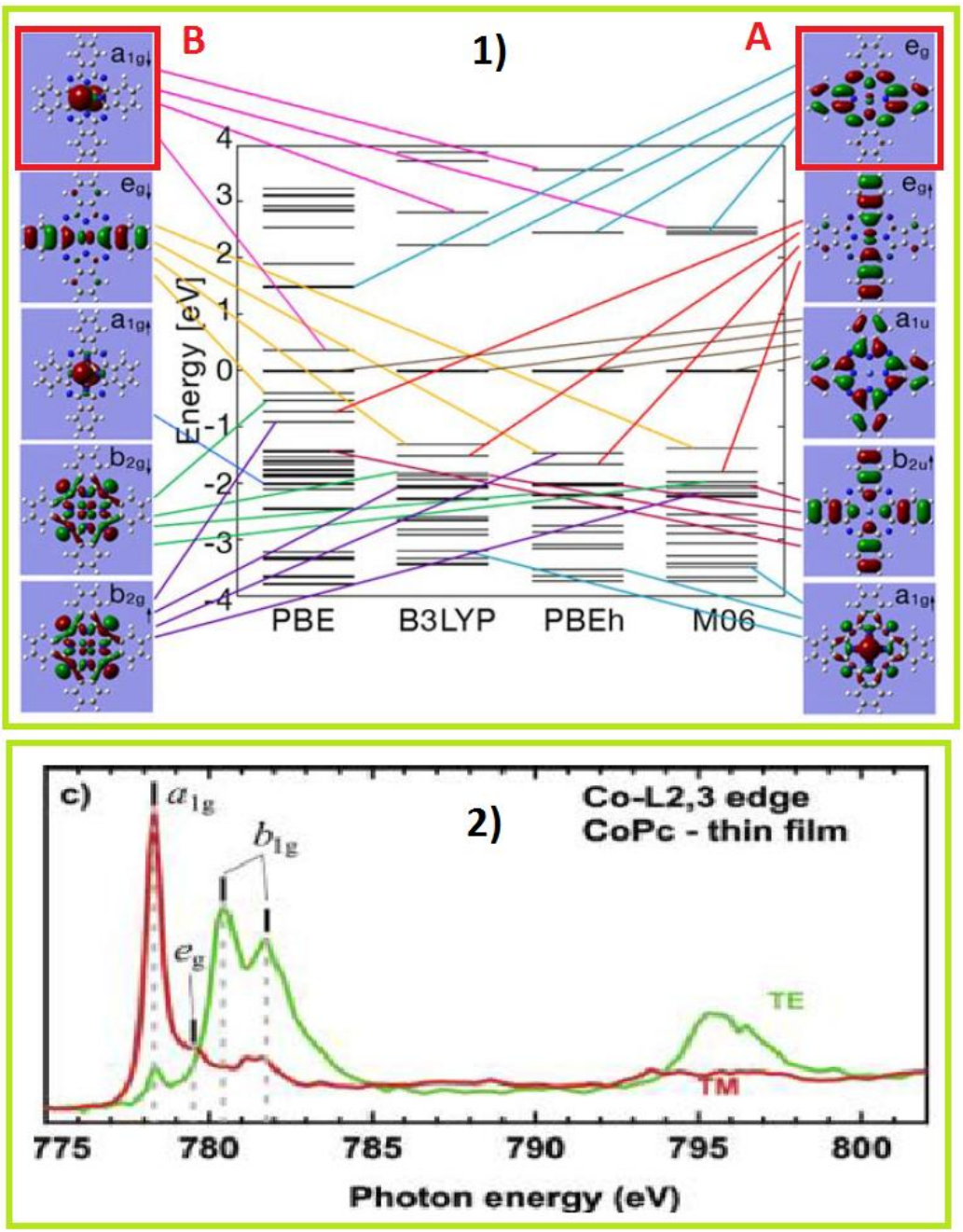

Figure 5.7. DFT calculations of single CoPc molecule, side pictures show the shape of the corresponding orbitals and point to their energy position in the calculated band structures, the red-green contrast is for visual help [29]. Bottom - Co L-edge XAS of CoPc film on Au (110) at different light polarization with respect to the surface [28].

In Fig. 5.7, (top) it is clearly visible how the different DFT correlation functionals (PBE, B3LYP, PBEh, M06) are generating different energy values for the same electronic states, making a direct comparison of experimental data with theoretical calculations difficult. Figures on the side of Fig. 5.7 (top) are displaying the localization of different electronic states within the CoPc molecule. To explain the

spectrum from the gas phase, it is also necessary to compare it to the spectrum of the ordered film of CoPc molecules on the Au(110), measured in two different geometries: with light polarization grazing (TE) to the surface and normal to it (TM). In this way it is possible to distinguish the out of plane molecular levels and the in plane molecular levels.

The two spectra are shown in Fig. 5.7 bottom. The green (marked TE) spectrum is taken with the light polarization vector parallel to the surface. Thus one can only see the in plane orbitals like the b_{1g} (d_{x2-y2}) (see Fig. 5.2) which indicates that the assignment in Fig. 5.6 is correct, the slight shift between the two b_{1g} peaks from XAS on film and XAS in gas phase can be attributed to the influence of interactions with the surrounding molecules and/or the substrate. The red (marked TM) spectrum (Fig. 5.7, bottom) is acquired with the light polarization vector orthogonal to the surface and is thus sensitive to the out of plane orbitals, such as the e_g ($d_{xz}d_{yz}$) and a_{1g} (d_{z2}) (see Fig. 5.2), whose corresponding peaks can now clearly be seen. However there is a difference between the gas phase spectrum (Fig. 5.6) and the red (TM) spectrum in Fig. 5.7: in the case of the film the shoulder corresponding to the e_g state is found after (at higher energy) the peak of the a_{1g}, which is not in agreement with any of the DFT calculated data, where it is always appearing at lower energies. The reason is that, for molecular films, the out of plane orbitals are responsible for the bonding of molecules to the surface: in this process the D_{4h} symmetry is in fact slightly altered and the energies of the states are changed, resulting in the reverse order of a_{1g} and e_g for the two cases [57].

With the comparison of the gas phase spectra to both the DFT calculations and the film measurements we can distinguish the real order of the unoccupied molecular orbitals related to the Co atom e_g, a_{1g} and b_{1g} in the gas phase, the data are also a good reference for future comparison with more consistent simulations of CoPc band structure. This data will also be a good reference for future pump probe experiments which are also mapping the unoccupied states.

5.5 Nitrogen K-edge XAS

The nitrogen K-edge XAS was acquired by using the same partial electron yield detection technique, as in the case of cobalt L-edge XAS. In this case the energy window was tuned on the Auger electrons of the nitrogen KVV transition. The monochromator was set to achieve a photon resolution of approximately 100 meV. In the XAS spectrum of Fig. 5.8 it is possible to recognize five main features: the first resonance (A) at 398.6 eV photon energy, the second resonance (B) at 401.1 eV, the third (C) at 402.6 eV and the fourth (D) at 406.3 eV. After the resonance E we can see a raising shoulder F indicating a structure beyond our measurement range. In order to properly describe the structure of gas phase N K-edge XAS we will again use the comparison to the XAS measurement of molecular CoPc films [28].

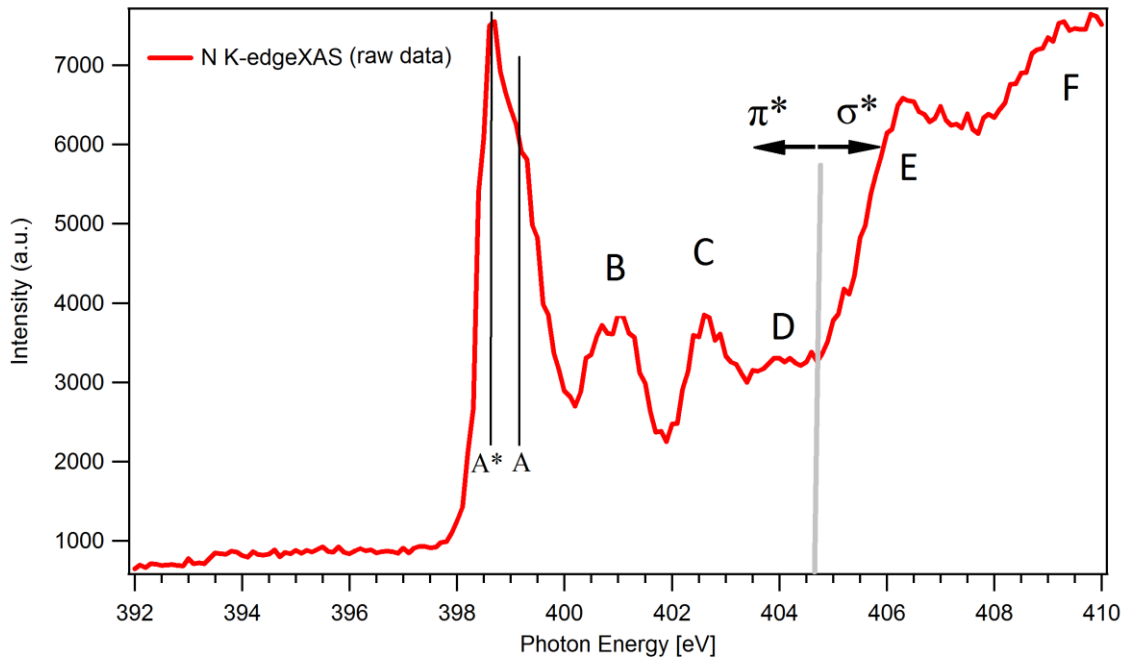

Figure 5.8, XAS of N K-edge in gas phase, A*,A ,B ,C ,D are the features due to $\pi*$ type orbitals, while E and F come from $\sigma*$ type orbitals.

Since the XAS transitions are sensitive to the orientation of orbitals with respect to the light polarization, one can in the case of ordered molecular films be sensitive to either $\pi*$ and $\sigma*$ molecular orbitals. By comparing the spectra in Fig. 5.8 to the spectra in Fig. 5.9 one can separate the structures due to the out of plane $\pi*$

contributions A, B, C D, and the in plane $\sigma*$ contribution, E and F. The first split peak can be deconvolved into two components A and A*, the latter being due to the transition from N 1s orbital of the pyrrole N atoms (N1 in Fig. 5.1) to the delocalized states $\pi*$ LUMO of the pyrroles. The second peak A is due to transition from bridge N atom (N2 in Fig. 5.1) to the same $\pi*$ LUMO delocalized states of the pyrroles. This is confirmed by the fact that the distance between the peak A* and A (~0.5 eV) is the same as the binding energy difference between the two components observed in N 1s XPS (Table 5.2) spectrum. The features B, C and D are due to transitions from N 1s to the out of molecular plane $\pi*$ type LUMO+n states of the pyrrole rings, while the features E and F are due to in molecular plane $\sigma*$ type LUMO+n states.

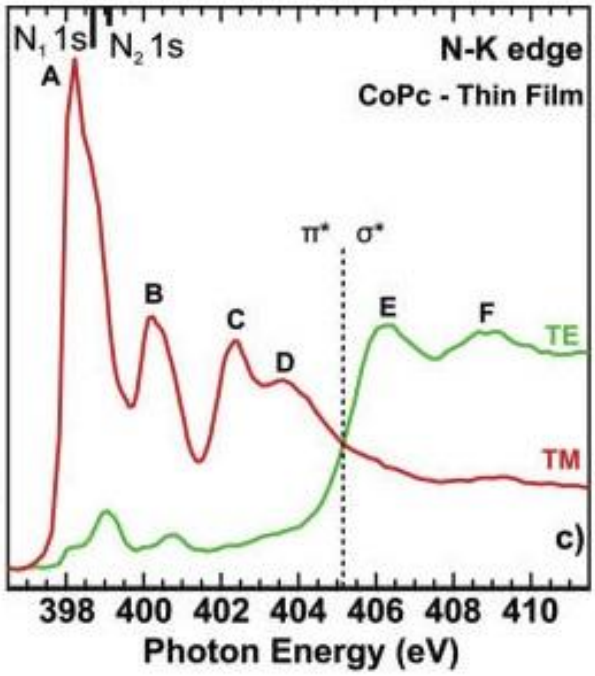

Figure 5.9, CoPc N K-edge XAS at different light polarization with respect to the surface, the acquisition was done with the in the same way as the CoPc XAS reported in Fig. 5.7 [28].

The data of N 1s XAS are an insight into the structure of the unoccupied states related to nitrogen atoms, and will be used for comparison to future pump probe experiments, as well as a comparison with single molecule and theoretical calculations for films.

5.6 Valence spectra

Valence spectra were measured using the same apparatus as for the XPS experiments. Measurements were performed at different photon energies, ranging from 28 eV to 150 eV. Some valence measurements were periodically repeated during the experiment, in order to check the stability of evaporation conditions. In the process of heating the molecules, water contamination was also monitored by means of valence photoemission, since its features are easy to detect due to their characteristic structures in the spectrum.

Valence spectra were primarily acquired to investigate the cobalt 3d orbital configuration in the gas phase, as well as the contributions from carbon and nitrogen atoms. Cobalt 3d electrons are the responsible for the conducting properties in thick films, and the fact that the 3d shell is not fully filled is also responsible for ferromagnetic properties of the cobalt atom and for the creation of chemical bonds to the neighboring atoms.

Thanks to the good resolution in electrons analysis of the ULLA end-station, and to the well focused and narrow bandwidth photon beam of the Gas Phase beam line, we have been able to acquire well resolved UPS spectra. The overall resolving power in our PES experiment was higher than 1000 for all photon energies in the 20-200 eV range, in order to obtain as much information as possible on the electronic structure of CoPc valence.

The valence spectrum of CoPc has been already measured by M. Vogel et al. with a He I (21.22eV) UV source [39]. Their result is shown in Fig. 5.10 (green plot) in comparison with the results of the theoretical models done by E. Salomon et al. [30], in an effort to attribute the corresponding peaks to the different Co 3d levels. The results of two G_0W_0, based models and two DFT (PBEh, PBE) functionals are also shown in Fig. 5.10. Due to the self-interaction errors (SIE) at DFT level, also manifested in the G_0W_0 calculations, the models are displaying different results with respect to each other [30]. These discrepancies prevent a precise and correct assignment of the Co 3d levels.

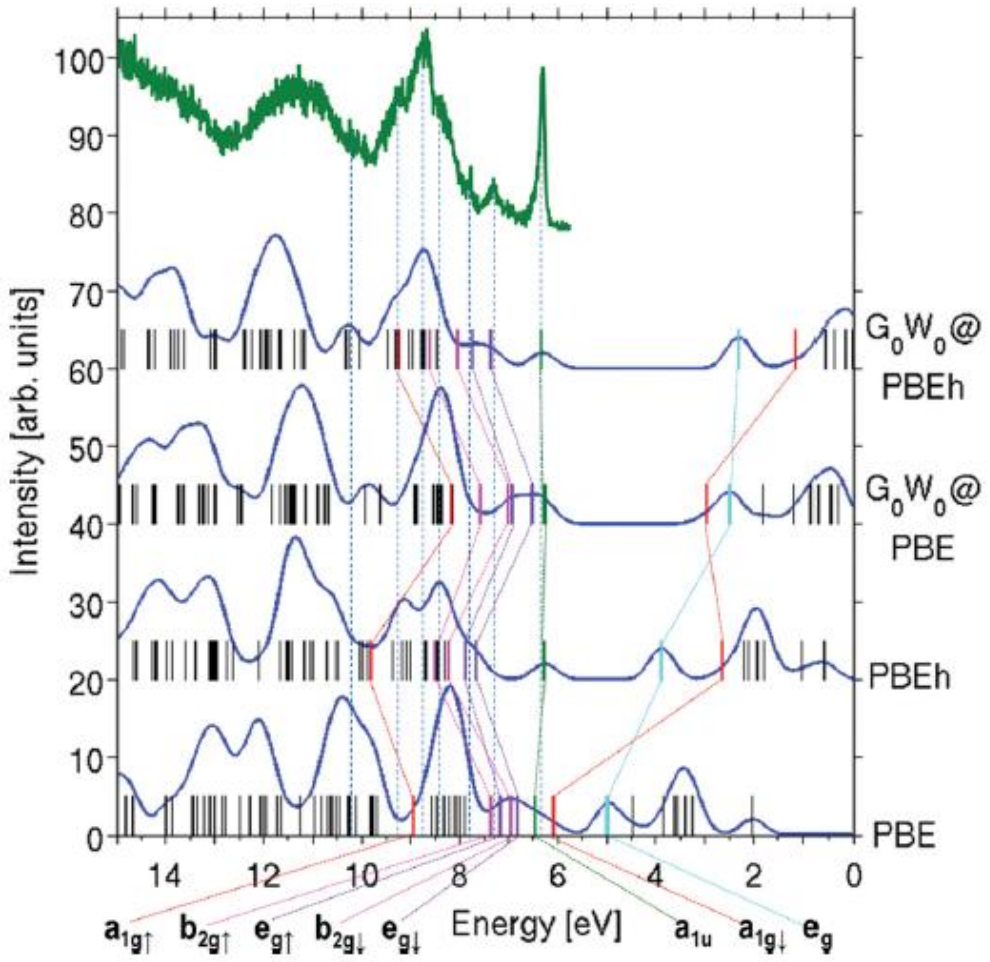

Figure 5.10, Gas phase spectrum of CoPC taken with He I, UV source (green). Valence PES calculations using different GW and DFT approaches. States a_{1g}, b_{2g} , $e_{g,}$, b_{1g} and their spin component are belonging to the Co 3d subshell, while a_{1u} is the HOMO orbital belonging to the benzene and pyrrole hybridizations, a_{1u} is the reference on which all the presented calculations are aligned [30].

In order to address better this issue we have performed valence photoelectron spectroscopy at high resolution and at different photon energies. Our experimental result are showing detailed features, as can be seen in Fig. 5.11. The spectra we have recorded at the gas phase beam line are providing more information than the spectrum presented in Fig.5.10 (green), because we could exploit the effects of different atomic ionization cross sections, thanks to the tunability of the photon energy.

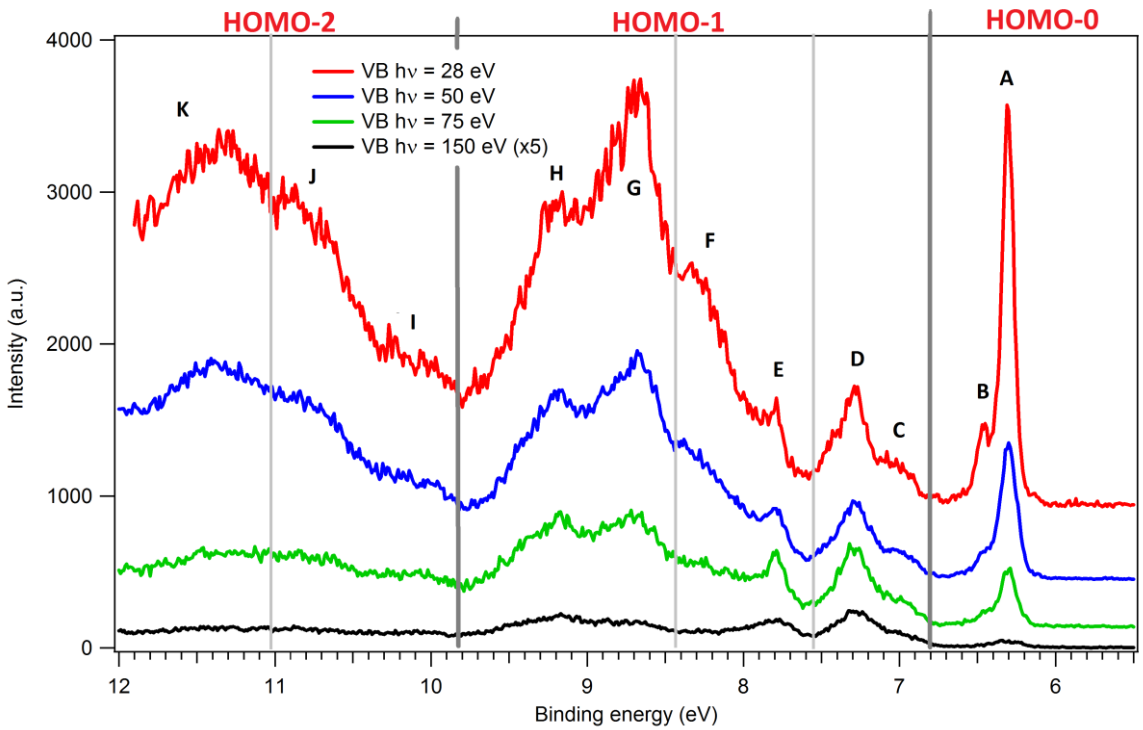

Figure 5.11, Gas phase CoPC valence spectra taken at the gas phase beam line. In order to characterize the ionization cross sections vs. photon energy, the spectra were acquired at different photon energies.

In the Fig. 5.11 we report four different photon energies ranging from 28 eV to 150 eV. All the spectra were calibrated in energy with the argon 3p peaks at 15.94 eV and 15.76 eV binding energies. The overall resolution was estimated by fitting the most intense argon peak (excluded from the plot) with a Voigt profile and extracting the FWHM value. As expected, the overall instrumental resolution (beam line + analyzer) of the measurements varies with the photon energy as is reported in Table 5.4:

Table 5.4 Photon energy and the corresponding overall (photon+anayzer) resolution.

Photon energy (eV)	Resolution (meV)
28	33
50	55
75	60
150	130

To guide the eye, the valence spectra have been sectioned in the same way as in [40]. The spectrum shown in Fig. 5.11 is divided into HOMO-0 (Highest Occupied Molecular Orbital), HOMO-1 and HOMO-2 orbital contributions. While all the observed spectral features were marked with letters from A to K.

UPS spectra performed at different photon energies are helpful in determining the various atomic orbital contributions to the valence electron density. As a rule of a thumb, components related to the lighter atoms, like N and C, have a higher ionization cross section at lower photon energies, while features related to the heavier Co atom are expected to have higher relative ionization cross section at higher photon energies.

From the calculations presented in Fig. 5.10, the exact positions of the occupied Co 3d levels cannot be extracted, while all calculations were consistent only in determining the energetic order of the occupied levels, $a_{g1\uparrow}$, $bg_{2\uparrow}$,$e_{g\uparrow}$, $b_{g2\downarrow}$, $e_{g\downarrow}$.

The first HOMO-0 peak A is well defined in all the models shown in Fig 5.10, and it is attributed to a_{1u} molecular orbital coming from the C-C and C-N hybridized $\pi*$ type orbitals [41]. We believe that the small feature B is also caused by the carbon and nitrogen contribution, since it is quickly disappearing when photon energy increases. Also feature F disappears at higher photon energies. For this reason we attribute it to orbitals related to the organic part of the molecule, i.e., carbon and nitrogen compounds. On the contrary, we believe that the features C, D, E, G and H correspond to 3d molecular states of cobalt (Fig. 5.9). C can be attributed to the spin down component of the doublet state e_g, D to the spin down component of the b_{2g}, E to the spin up splitting of the e_g state, and finally the spin up components of the b_{2g} and a_{1g} are attributed to the features G and H. The positioning of the a_{1g} spin up feature is particularly interesting since it is responsible for the non-zero net spin of the molecule. Since the spin down component of a_{1g} lies in the unoccupied orbitals, as results from the study of the Co L-edge XAS, the net spin for the cobalt atom embedded in the CoPc molecule is S=1/2.

Finally the HOMO-2 with its components I, J, K consists of σ benzene and pyrrole carbon states [42]

From the valence spectra and the current calculations of the electronic structure, using the DFT [43] it is still not possible to correctly assign all the energy levels. So, in order to confirm the assumptions on the assignment of Co related states in the valence spectrum, further resonant photoemission investigations, on cobalt core levels, are necessary. In this way it will be possible to distinguish the contributions due to the resonant atomic species.

Valence spectra presented in this Chapter are a step forward to a proper assignment of the occupied electronic levels present in the CoPc valence. By combining them with the complementary XAS measurements it is possible to gain an insight into both occupied and unoccupied levels of the CoPc molecule.

6 Commissioning of LKO setup and preparation of Au(111) surface

As already mentioned, phthalocyanines are particularly interesting when deposited on a substrate, in thin molecular films. Phthalocyanines on surfaces have been widely studied with conventional spectroscopic techniques at high energy resolution or high spatial resolution or momentum resolution [8, 11, 12, 28]. However, state-of-the-art modern characterization techniques are also capable of providing time resolution at the same temporal scale of electronic processes in solids, i.e. the femtosecond scale.

In order to investigate material properties on a very short temporal scale, in our case in the range from pico to tens of femtoseconds, it is mandatory to use a probe characterized by short light pulses, in the range of the soft X-rays, possibly tunable in wavelength. A light source of this kind has recently been implemented at the Laboratory of Quantum Optics in University of Nova Gorica and will be primarily used to perform time resolved photoemission experiments on surfaces.

The choice of the specific Au surface is related to the fact that it is the perfect benchmark to check the performances of the light source and the experimental chamber, thanks to its well known surface state.

The purpose of the experiment presented in this Chapter is to contribute to the commissioning of photoemission setup and of the experimental chamber. The long-term goal will be to study the interface of the PcCo on Au(111) substrate.

6.1 ARPES

Angular resolved photoemission spectroscopy (ARPES) is a key technique to study electronic properties of surfaces. Going back to the description of photoemission provided in Chapter 3, the equation of simple energy conservation can be reused for the particular case of photoemission from solid:

$$E_{kin} = \hbar\omega - E_b - \phi_0, \tag{6.1}$$

Where E_{kin} is the kinetic energy of the outgoing electron, E_b is the binding energy of the electron in its initial state relative to the Fermi level and ϕ_0 is the work function of the surface (energy required for an electron to escape from the solid).

In low energy PES the photon momentum is negligible if compared to electron momentum. For total momentum conservation, in the case of smooth surfaces, translational symmetry requires that the component of electron momentum in the plane of the sample to be conserved, i.e $k_{||inside} = k_{||outside} = k_{||}$, where

$$k_{||} = \frac{\sqrt{2mE_{kin}}}{\hbar}\sin\vartheta \tag{6.2}$$

where ϑ is the emission angle from the solid.

Relation 6.2 allows to determine the parallel momentum of the electron from the two measured quantities E_{kin} and ϑ. In Fig. 6.1 a typical ARPES set up is sketched from geometrical point of view.

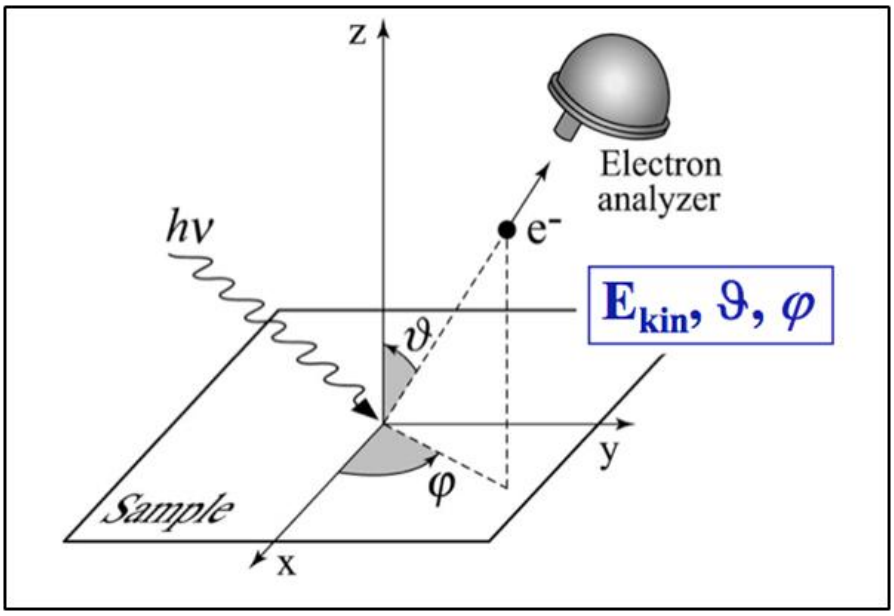

Figure 6.1, schematic view of an ARPES experiment, where the E_{kin} is kinetic energy, φ is the azimuthal angle, ϑ is the polar angle under which electron is emitted. [47].

6.2 Au (111) surface state

In order to commission our apparatus devoted to surface science, the test sample of Au (111) needs to be prepared in situ, in order to get an atomically clean and reconstructed surface. The ultimate proof of the surface quality is the presence of a surface state, which will be measured by means of ARPES.

One of the most basic concepts of solid-state physics is the Bravais lattice. By definition, a Bravais lattice is an infinite periodic array in which the repeated units of the crystal are arranged. These units may be single atoms or molecules [26]. Thus a Bravais lattice is the description of an ideal crystal. In nature however all the crystals exhibit distortions of periodicity and imperfections. Also the surface can be seen as a break of the perfect three dimensional symmetry, generating the region of contact with the surroundings, in our case the vacuum. On the surface it is possible to observe new phenomena and physical features, like the formation of an electronic surface state [44].

In general, calculations of the electronic band structure are based on the one-electron approximation, i.e. one electron is assumed to be embedded in the periodic ionic potential, plus an averaged constant field due to other electrons, which replaces the individual pair potentials. In addition, one neglects nuclear motions and assumes fixed ionic potentials (Born–Oppenheimer approximation). The solution of the corresponding one-electron Schrödinger equation gives the well-known Bloch solution [26]**.** If the crystal is terminated by a surface, the electron wavevector ***k*** may also assume complex values and one gets energy eigen values that lie inside the energy gaps of the infinite crystal. Due to the imaginary part of the wavevector component perpendicular to the surface, $k_{\perp}$, these new states are monotonically damped in the direction of the vacuum and also damped, but still oscillating, in the direction towards the bulk of the crystal. Consequently, these states are localized at the crystal surface [45]. Therefore, surface states play an important role for the dynamics of surface or interface related processes, such as adsorption, catalysis and, chemical reactions at surfaces [46, 44].

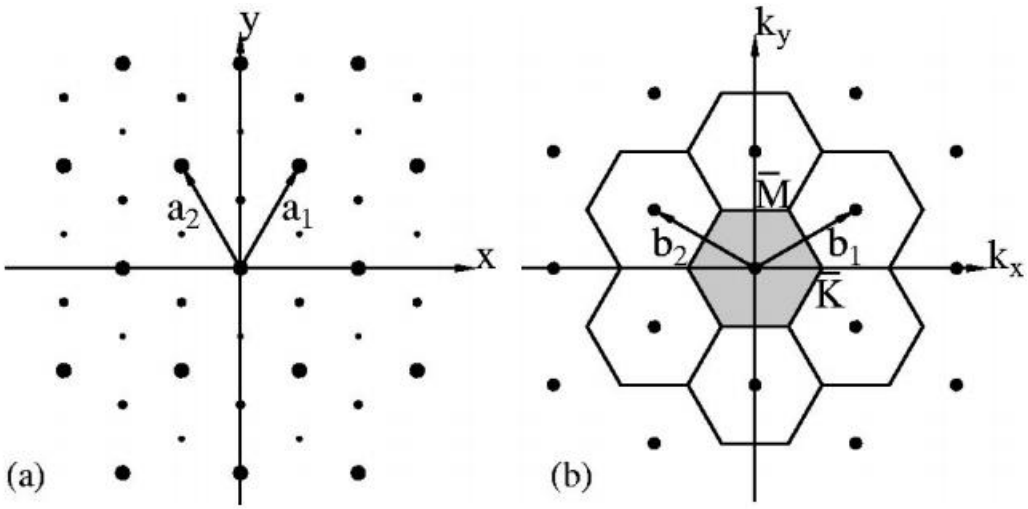

Figure 6.2. The Au(111) surface (a) Top view of the first three layers depicted by large, medium and small dots, $\mathbf{a}_1$ and $\mathbf{a}_2$ are the basis vectors of the lattice, (b) an image of the two dimensional reciprocal lattice with the basis vectors $\mathbf{b_1}$ and $\mathbf{b_2}$, the high symmetry points $\bar{M}$ and $\bar{K}$, gray hexagon is the unit cell in the reciprocal lattice called the first Brillouin zone [26, 50]

The Shockley surface states of Cu, Ag, Au (111) crystals have been extensively studied during the last 20 years [48, 49, 50, 51, 52]. They are characterized by a

parabolic dispersion of energy versus momentum. The value of the Fermi momentum became a good reference to characterize energy and momentum resolution and linearity of the detector. A gold single crystal of has cubic face centered symmetry (FCC). The surface generated along the (111) direction has the crystal structure shown in Fig. 6.2.

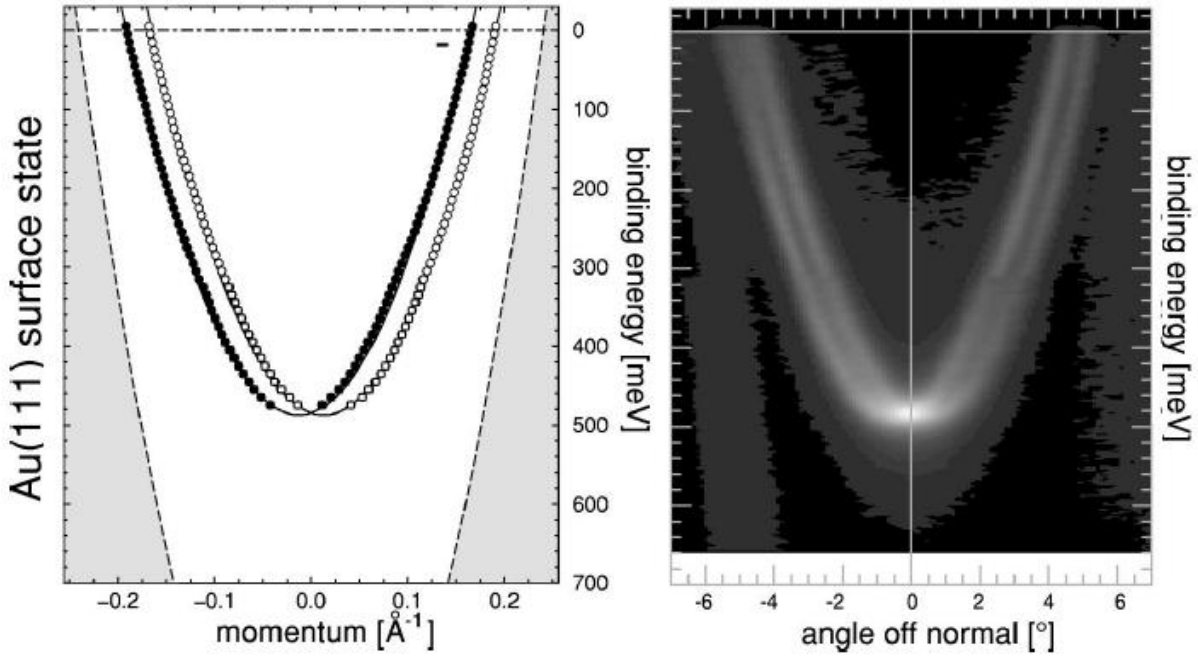

Figure 6.3. Right-calculated dispersion of Au(111) surface state. Left – experimental data with the He I UV source [52].

For a clean reconstructed surface, the resulting surface state is looks like the one in Fig. 6.3 (left), the image is from F. Reinert et al. [52]. On the left figure is visible the dispersion of the surface state as a function of binding energy. The right image of Fig. 6.3 shows a high resolution ARPES measurement of the Au(111) surface state using a helium discharge lamp ($h\nu = 21.22eV$). Note that both images in Fig. 6.3 show a splitting in momentum. This is due to a phenomenon called the spin splitting of surface state, and is a consequence of the spin-orbit coupling in the surface state [49, 50]. Due to the fact that the expected overall energy resolution of our light source is about an order of magnitude lower than the resolution of the measurement shown in Fig. 6.3, we do not expect to observe the splitting.

6.3 Experimental setup

In order to observe the surface state one needs an experimental setup that provides ultra high vacuum conditions, in situ sample preparation, a light source with sufficiently narrow photon bandwidth and an electrons' analyzer, with sufficient energy and angle resolution.

6.3.1 Pump probe time resolved experiments

Time resolved experiments are performed in order to investigate events occurring at a very short temporal scale of femto and picoseconds. In this temporal scale one can observe processes like electronic transitions, chemical reactions etc. In order to measure such dynamic events use is made of the "pump probe" technique. This technique requires two ultra short pulses with a tunable delay. The first pulse the "pump" is used in order to initiate the investigated transition, reaction, etc., by exciting the system into an out of equilibrium state. The second pulse, the "probe" investigates the properties of the system after a certain delay. By performing a sequence of measurements at different delay one can obtain the dynamics of the relaxation process of the investigated system.

6.3.2 The light source

Modern commercially available lasers are able to generate extremely powerful visible and infrared pulses with time duration in the femtosecond range. In order to make them useful in the field of photoemission spectroscopy, these pulses need to be tunable in the range of ultraviolet (UV) and extreme ultraviolet (XUV). This becomes possible if lasers are used to generate high order harmonics (HHG) in gas.

In a HHG process using a noble-gas, atoms interact with an intense laser field and emit light at the harmonics of the laser frequency. The process can be described by means of a semi-classical "three step model" [53]. In the first step, a bound electron is extracted from a gas atom under the action of the laser field; in the second step, the electron undergoes an oscillating motion imposed by the laser field; in the third step, the electron collides back with the parent ion. As a result, laser harmonics are emitted up to wavelengths extending into the soft X-ray regime [54]. A spectrum of the HHG generation process is shown in the insert of the Fig.6.4.

HHG is implemented at the CITIUS facility hosted by the Laboratory of Quantum Optics at the University of Nova Gorica (Slovenia). CITIUS is a laser based light source devoted to ultrafast scientific investigations.

The CITIUS laser system and the beam line are schematically shown in Fig. 6.4. The laser system comprises a commercial amplifier Legend Elite Duo and an optical parametric amplifier OPerA (OPA), both produced by Coherent Inc. The amplifier is seeded by a Micra oscillator (wavelength: 800 nm, spectral bandwidth about 100 nm, power about 380 mW) and includes two amplification stages: a regenerative amplifier (EVO 30), pumped by an Evolution 30 laser (frequency-doubled Q-Switched Nd:YLF laser), and a single-pass amplifier (EVO HE), pumped by an Evolution HE laser (frequency-doubled Q-Switched Nd:YLF laser). The system can be operated at four different repetition rates: 100 Hz, 1 kHz, 5 kHz and 10 kHz. At 5 kHz, which is the currently adopted repetition rate, it generates pulses carrying about 3.1 mJ, with a duration of about 35 fs, centered at 805 nm. Two thirds of the energy is used for generating XUV pulses through HHG, one third as a pump for the OPA, or directly in combination with the HHG beam for pump-probe experiments. The OPA produces tunable radiation in the range between 0.4 eV and 5.6 eV, with variable energy per pulse (from few to hundreds of microjoules). The optical elements transporting the fundamental have a roughness equal to $\lambda/6$. The beamline includes a high-vacuum section, through which the XUV beam propagates, and a section in air, used to transport the IR-UV light generated by the OPA. The XUV part comprises a HHG generation chamber and a monochromator. The laser is focused in the generation chamber , where it interacts with a noble gas of choice (Ar or Ne, for the reported experiments) contained in a cell, generating the high-order harmonics. The harmonic

generation efficiency can be optimized by varying the laser intensity, the gas pressure (typically, of the order of 10^{-3} mbar) and the relative position of the laser focus within the cell [54].

The peculiarity of the beam line is a double configuration monochromator, which allows one to operate either at high temporal resolution, using a set of conical gratings mounted in a so-called off plane geometry, or at high energy resolution, using a conventional set of gratings mounted in a classical geometry.

The two beams generated by OPA and HHG are recombined in the "recombination chamber" and focalized in an almost collinear geometry on the sample.

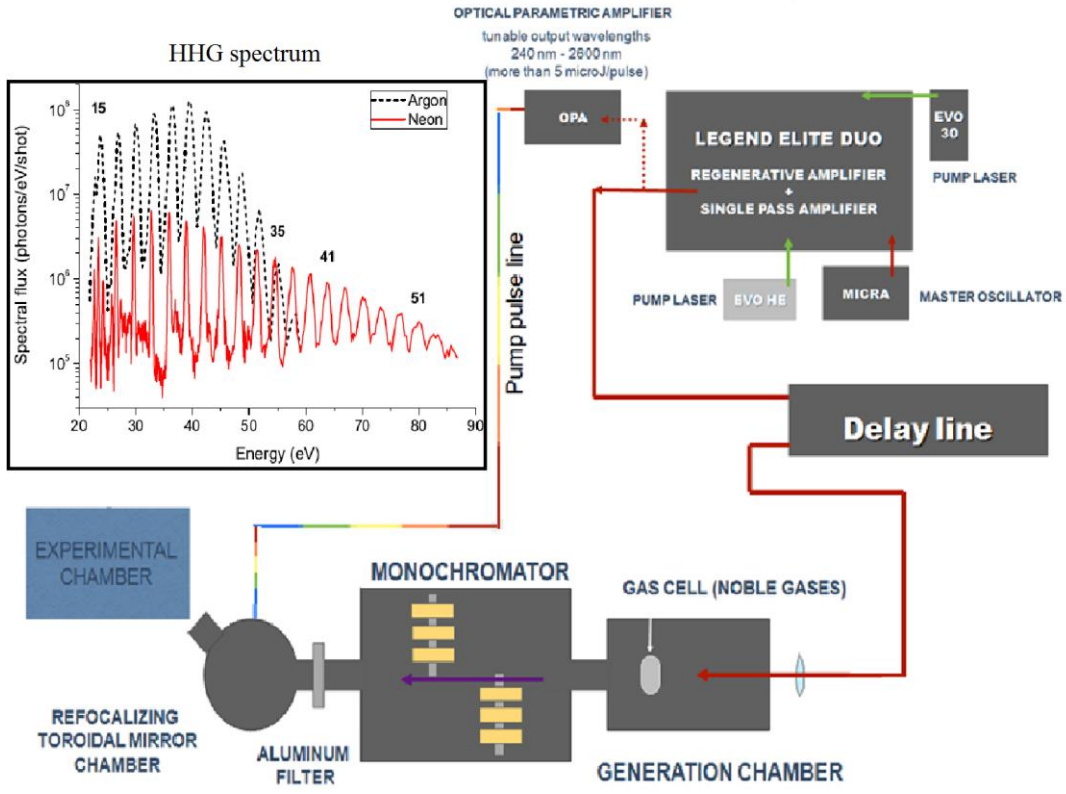

Figure 6.4. CITIUS lightsource layout: the pump lasers (Evo 30, Evo HE), the Micra master oscillator, the Legend elite amplifier, the generation chamber, the monochromator and refocalization mirror chamber. Top left- spectrum of the HHG generation in argon and neon

The final output power of the laser amplifier was limited to 0.5 mJ per pulse instead of standard 3.1 mJ due to technical problems. Measurement of the harmonics intensity revealed that in this configuration the final intensity of the harmonics was at

least one order of magnitude lower. Thus the exit slits of the monochromator needed to be fully opened trading resolving power for photon flux.

6.3.3 Experimental chamber

The experimental chamber is realized in μ-metal, a specific alloy for UHV applications that shields residual magnetic fields, like earth magnetic field and those induced by the devices and equipment in the laboratory. To reduce the fields due to the magnetic levitation turbomolecular pump, the pump is placed on the bottom of the chamber far from sample position. Vacuum is maintained also by a Titanium-Sublimation Pump (TSP) [55] mounted inside a large liquid nitrogen trap. The trap is used for rapid vacuum recovery after processes like annealing or sputtering (see Section 6.4). Normal operation pressure of the system is in the range of 10^{-10} mBar.

The chamber has a multiple-flange design. It hosts an argon ion sputter gun and a four-degree of freedom (3 translation, x y z and polar rotation) manipulator. The sample holder stage allows electron beam heating. In this process electrons are extracted from a filament using thermoionic emission. Electrons are then accelerated by a high voltage bias towards the back of the sample plate. The impinging of these highly energetic electrons on the sample plate increases the temperature. This technique allows to reach temperatures up to 1000°C on the sample.

The chamber is equipped with and XR6-monochromatized X-ray source (from ThermoScientific) generating photons from the Al K_α lines at 1486.7eV. The ultimate resolution of the X-ray source is around 350 meV. The hemispherical electrons analyzer is a Scienta R3000. It has an energy resolution from 3-30 meV in the photon energy range of our HHG source.

The spectrometer can work either in transmission mode for XPS or in angular dispersion mode for ARPES. It is possible to select four angular modes (±3°, ± 5°, ±7.5°, ±10°), with the ultimate angular resolution of 0.1° for light sources' spot in the

0.1 mm range [56]. The analyzer can measure electrons with energies from 0.5 up to 1500 eV, which makes it the ideal instrument for use with both the laser source and the X-ray source. In future the plan is to use it also with an He discharge UV source in order to perform conventional ARPES to characterize the system before proceeding to pump probe experiments.

In order to be able to introduce samples into vacuum without venting the whole system the chamber has a small fast entry chamber, which is separated from the main chamber by a valve. This chamber is equipped with its own pumping system and pressure gauge. This smaller chamber will also be used to prepare films of CoPc molecules deposited on gold in near future.

6.4 Sample preparation

The presence of a surface state depends on the quality of the surface. The surface needs to be well ordered and clean on the topmost atomic levels. A sample exposed to air absorbs oxygen and water molecules from air as well as other contaminants, during storage, cleaning and mounting procedures. To get an atomically clean and reconstructed surface, several cycles of sputtering and annealing were performed repetitively for few days.

The sample is a 2 mm thick disc of gold single crystal with 8 mm diameter. The top surface of the disc shown in Fig. 6.5 is the Au(111) surface. The sample is mounted on a molybdenum sample plate, which allows the use of electron bombardment heating.

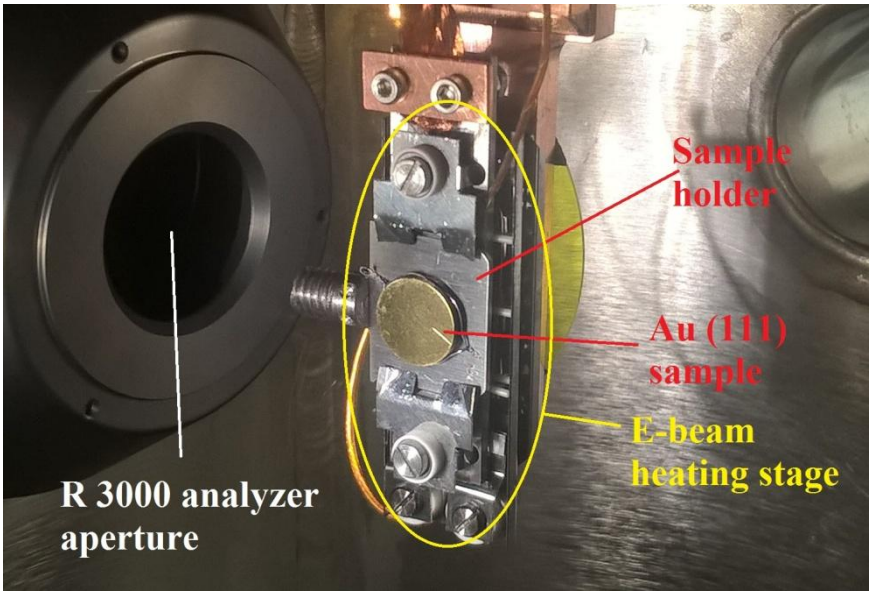

Figure 6.5, Au (111) single crystal on a molybdenum sample holder, inserted into the e- beam heating stage. The entire assembly is mounted inside a UHV chamber.

Once the sample is inserted into vacuum the whole assembly (molybdenum sample plate and Au single crystal) was degassed, as the vacuum was left to stabilize at the base pressure of 6×10^{-10} mBar. Before carrying out any cleaning procedures XPS spectra using the Al K_α X-rays were taken in order to determine the elemental structure of the surface. The red spectrum shown in Fig. 6.7 is displaying the XPS overview of Au (111) surface before the cleaning procedure: stronger peaks are due to gold, while there is a clear presence of C 1s peak indicating contamination with organic molecules. Spectra acquired in binding energy range of the O 1s (not shown) reveal also the presence of oxygen and water contamination.

After the spectrum was acquired the sample was sputtered. Argon ion sputtering is a process of surface bombardment with argon ions accelerated using high voltage. In this ballistic etching process the topmost atomic layers containing contaminations are removed. After the sputtering the XPS measurement was repeated (green spectrum, Fig. 6.6), the C 1s peak disappeared as well as the O 1s and a clear increase of signal from all the gold core levels was observed.

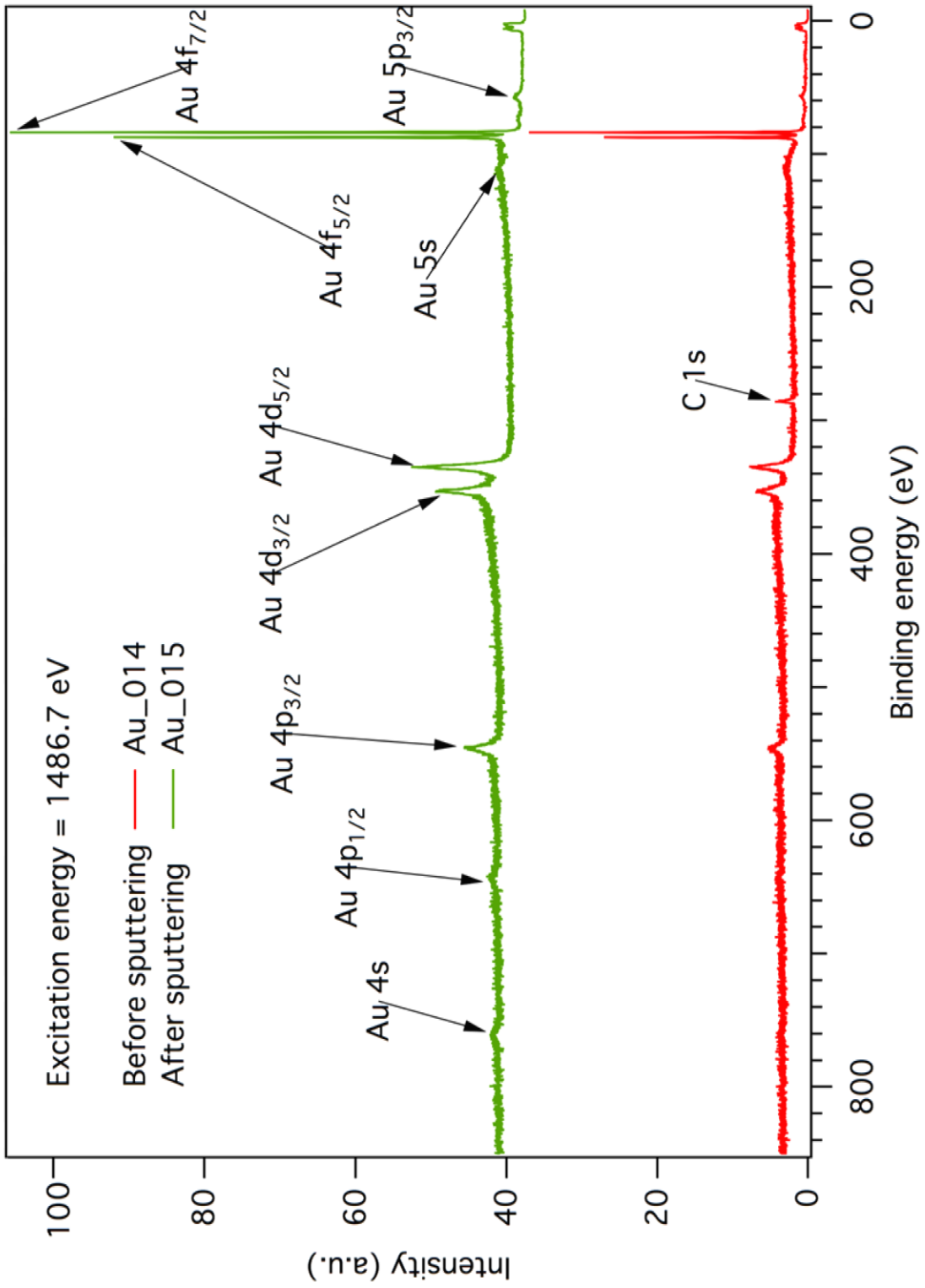

Figure 6.6, XPS overview of Au(111) surface before (red) and after (green), the sputtering procedure, the tags are marking the contributions from different gold and carbon core levels.

After the sputtering procedure the contaminants were removed from the surface, however the aggressive process of sputtering also removes the gold atoms from the topmost layers of the crystal leaving a rough surface. In order to reconstruct the crystalline surface the sample gold must be heated above 500°C to let the gold atoms rearrange and reconstruct the surface. The process depends on the performance of the heating stage, the thickness and size of the sample, the quality of vacuum and the ability of the operator to precisely control the temperature.

Finally, UPS and ARPES measurements were performed in order to check for the presence of the surface state.

6.5 ARPES study of Au(111)

As seen in Fig. 6.3 the surface state is a feature extending about 0.5 eV beneath the Fermi energy, in the angle integrated mode it can be seen as a small peak just behind the Fermi level. Before measuring a valence band spectrum, with a detectable structure corresponding to the surface state, closed to published data of the Au(111), the sample underwent several cycles of sputtering and annealing. The alignment procedure of sample and light was also repeated numerous times.

Figure 6.7 is displaying the first ARPES measurement acquired with this setup: the surface state appears shifted in angle by 3°, due to bad sample tilt angle, that could not be compensated with the manipulator. The alignment of the light, sample and analyzer was performed on the most intense peak of the Au valence band (see Fig. 6.7, A).

Angular dispersion of the surface state is visible as well as the *d bands* (the 2 features marked A and B). All the spectra were measured with the sample at room temperature.

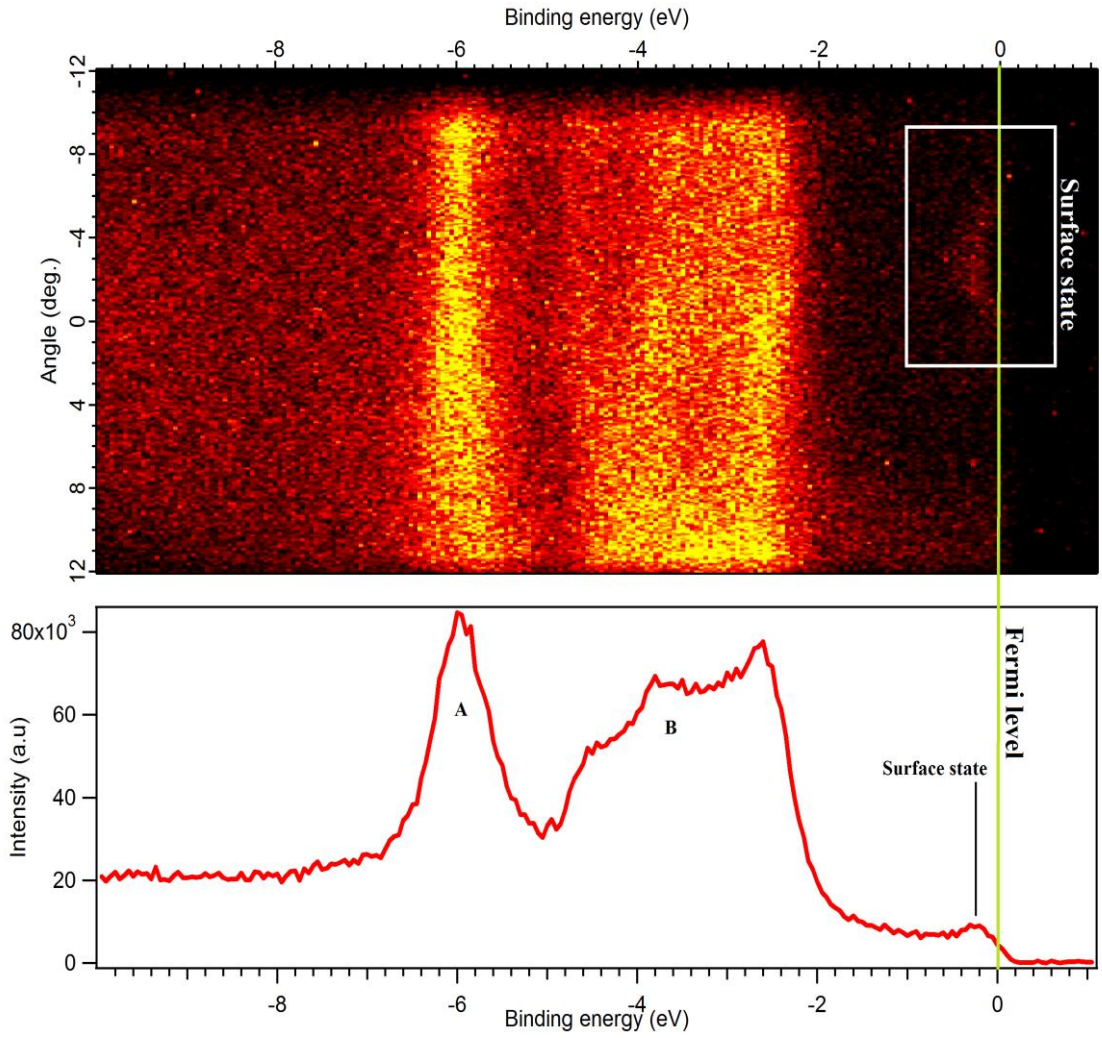

Figure 6.7, top-ARPES measurement of the Au(111) valence band measured at 31.5 eV photon energy, bottom- Angle integrated spectrum of the top image.

After the presence of the surface state was confirmed, a close up ARPES measurement of the surface state region was set.

The displayed ARPES spectra were measured at 31.5 eV photon energy. From the MDC (momentum distribution curve at $k = 0$ $Å^{-1}$, blue line marked MDC 1) it is possible to determine the minimum energy of the surfaces state 0.5 eV, in agreement with the theoretical values shown in Fig. 6.3 (left). The spectrum has been converted from angle of emission to $k_{||}$ using equation 6.2.

In Fig. 6.8, taking the MDC where the surface state crosses the Fermi energy (green line marked MDC 2) it is possible to estimate the values for the Fermi momentum ($k_{||}$ at Fermi energy) $k_F = 1.3\ Å^{-1}$, which is within our resolution in agreement with the values of Fig 6.3.

From the Fermi edge step of the spectra acquired during these experiments we can estimate that the overall energy resolution of the measurements was approximately 250 meV. The factors contributing to the spectral broadening are the analyzer settings (50 meV), the sample temperature, but the major effect is coming from the spectral width of the laser harmonics.

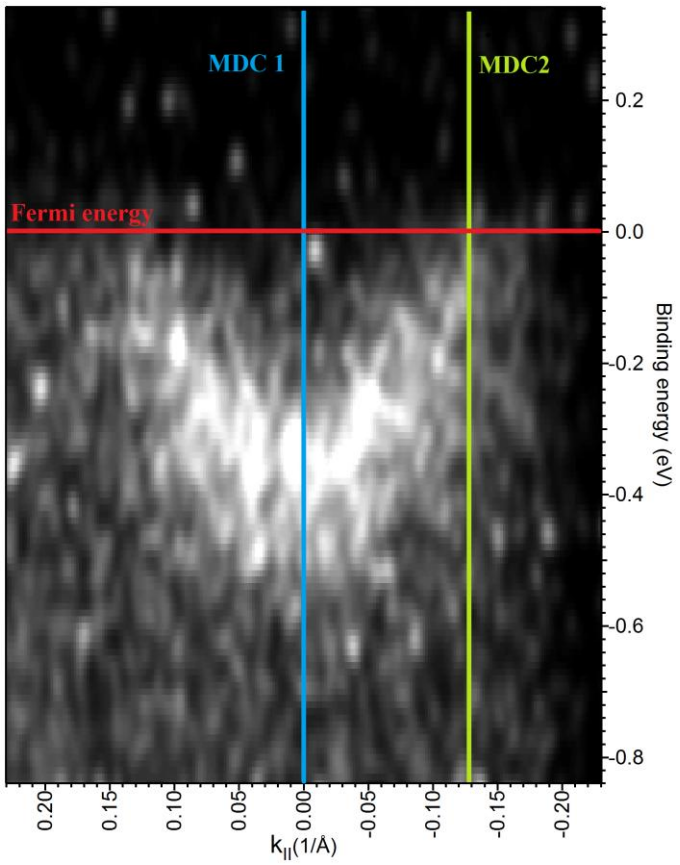

Figure 6.8, ARPES measurement of the Au (111) surface state measured with 31.5 eV photon energy, *k*-parallel was calculated from the electronic angle of emission.

It's worth to stress that this is the first set of data of the CITIUS photoemission set up. They are good for a qualitative evaluation. Because of the low performance of the laser during the experiments, the photon energy was selected in order to work on the

most intense harmonic with photon energy of 31.5 eV (21^{st} harmonic of the laser). In the near future the experiments will be repeated with the fully operational laser system, a better manipulator and a different electrons' spectrometer. In this improved configuration the resolution as well as the signal to noise ratio are expected to drastically improve.

The experiment presented in this Chapter is the first step in the commissioning of the CITIUS light source and the photoemission apparatus. The commissioning will continue with the experiments on the clean Au surface and on the CoPc interface in the time resolved setup.

7 Conclusion

In this thesis work the CoPc molecule in gaseous phase has been characterized using different kinds of investigation techniques.

By core level photoemission experiments we could determine that the structural properties of the molecules have not been altered by the process of high temperature evaporation. Also the splitting of the core level electron lines to several components, due to different chemical environment of carbon and nitrogen atoms, provides support to the expected chemical structure of the molecules. The results of Co 3p XPS enable us to determine the proper photon energy range for future investigation of valence band with resonant photoemission.

Valence spectra were measured to characterize the occupied electronic levels, with specific interest in the electronic configuration of Co 3d levels, which are responsible for the magnetic properties of the molecule.

By means of the XAS measurements we gained an insight into the unoccupied levels of the CoPc molecule, in particular the unoccupied levels related to the cobalt and nitrogen atoms. Recognizing the separate contributions from nitrogen and cobalt will be crucial for the data analysis in future excited state and pump probe experiments.

This work is a step forward to the full electronic characterization of the isolated molecule, and the characterization of dynamic processes on the films of CoPc molecules deposited on Au(111) surface, necessary for the implementation in real devices.

To this aim we carried out the first ARPES experiment on Au (111) surface state, using the new photoemission apparatus of the Laboratory of Quantum Optics at UNG.

References

[1] Non volatile memory: https://en.wikipedia.org/wiki/Non-volatile_memory.

[2] I. Bergenti, V. Dediu, M. Prezioso, A. Riminucci, Organic spintronics, Phil. Trans. R. Soc. A **369**: 3054–3068 (2011).

[3] M. Julliere, Phys. Lett. A **54**: 225-226, (1975)

[4] M. N. Baibich, J. M. Broto, A. Fert, F. Nguyen Van Dau, F. Petroff, P. Eitenne, G. Creuzet, A. Friederich, and J. Chazelas, Phys. Rev. Lett. **61**: 2472 – 2475 (1988)

[5] Elettra synchrotron facility: http://www.elettra.trieste.it/

[6] Gema de la Torre et al., Chem. Commun., **20**: 2000-2015, (2007).

[7] D. L. Ventura, C. M. Mazuca, Mild Synthesis of Metallophthalocyanines , Int. J. of Appl. Sci. and Tech. **4**: 149 (2014).

[8] Bidermane I., 2014 , Structure and Electronic Properties of Phthalocyanine Films on Metal and Semiconductor Substrates, Digital comprehensive Summaries of Uppsala Dissertations from the Faculty of Science and Technology 1119.

[9] M. G. Walter, A. B. Rudine, C. C. Wamser, Journal of Porphyrins and Phthalocyanines, **14**: 758-792 (2010).

[10] Y. Zhang et al., Struct Bond **135**: 275-321 (2009).

[11] Nilson, K. 2007 , Phthalocyanines on Surfaces. Monolayers, Films and Alkali Modified Structures, Digital comprehensive Summaries of Uppsala Dissertations from the Faculty of Science and Technology 342.

[12] J. Åhlund. 2007. Electronic and Geometrical Structure of Phthalocyanines on Surfaces, Digital comprehensive Summaries of Uppsala Dissertations from the Faculty of Science and Technology 291.

[13] J. Åhlund, J. Schnadt, K. Nilson, E. Gothelid, J. Schiessling, F. Besenbacher, N. Mårtensson, C. Puglia, Surf. Sci., **601**: 3661-3667 (2007).

[14] S.Hufner, Photoelectron Spectroscopy Principles and Applications, Springer (2003).

[15] G. Ertl, J. Kuppers, Low Eenergy Electrons and Surface Chemistry, VCH (1985).

[16] F.Reinert, S. Hüfner, New Journal of Physics **7**: 97 (2005).

[17] Auger effect: https://en.wikipedia.org/wiki/Auger_effect

[18] Summary of NEXAFS: https://www-ssrl.slac.stanford.edu/stohr/nexafs.htm

[19] Gas Phase beam line, homepage: https://www.elettra.trieste.it/elettra-beamlines/gasphase.html

[20] G. Turri, Study of electronic correlation in noble gas atoms by means of two electron photoemission spectroscopies, Dottorato di ricerca in fisica, Politecnico di Milano.

[21] C. Grazioli, et al. Rev. of Sci. Instrum. **85**: 23104 (2009).

[22] N. Martensson, P. Baltzer, P.A.Bruhwiler, J.O.Forsell, A.Nilsson, A. Stenborg, B. Wannberg, J. Elect. Spectr. Rel. Phen. **70**, 117-128 (1994).

[23] Carla Puglia et al., Elettra Experimental Report, proposal number 20115157, 2012.

[24] Photoelectron spectroscopy: https://de.wikipedia.org/wiki/Photoelektronenspektroskopie

[25] Y. Alfredsson, B. Brena, K. Nilson, J. Åhlund, L. Kjeldgaard, M. Nyberg5, Y. Luo, N. Mårtensson, A. Sandell, C. Puglia and H. Siegbahn, J. Chem. Phys. **122**: 214723 (2005).

[26] Neil W. Ashcroft, N. David Mermin, Solid State Physics, Brooks Cole (1976).

[27] P. Gargiani, G. Rossi, R. Biagi, V. Corradini, M. Pedio, S. Fortuna, A. Calzolari, S.Fabris, J.C.Cesar, N. B. Brookes, M. G. Betti, Phys. Rev. B **87**: 165407 (2013).

[28] M. G. Betti, P. Gargiani, R. Frisenda, R. Biagi, A. Cossaro, A. Verdini, L. Floreano, and C. Mariani, J. Phys. Chem. C **114**: 21638–21644 (2010).

[29] N. Marom, L. Kronik, App. Phys. A **95**: 159–163, (2009).

[30] E. Salomon, P. Amsalem, N. Marom, M. Vondracek, L. Kronik, N. Koch, and T. Angot, , Phys. Rev. B **87**: 075407 (2013).

[31] A. C. Thompson et al., X-ray Data Booklet, Lawrence Berkeley National Laboratory, Second edition, January 2001.

[32] V. Myrseth, J. Bozek, E. Kukk, L. Saethre, T. D. Thomas, J. Elect. Spectr. Relat. Phenom. **122**: 57 (2002).

[33] Y. Alfredsson et al., J. Chem. Phys., **122**: 214723, (2005).

[34] M. Schmid et al., Surf. Interface Anal. **46**: 505-511 (2014).

[35] M. Grobosch, C. Schmidt, R. Kraus, M. Knupfer, Organic Electronics, **11**: 1483-1488 (2010).

[36] I. Bidermane et al., Phys. Status Solidi (b) **252**: 1259–1265, (2015).

[37] T. D. Thomas, R. Shaw J., Electron Spectrosc. Relat. Phenom. **5:** 1081 (1974).

[38] L. Massimi et al., J. Chem. Phys. **140**: 244704 (2014).

[39] Michael Vogel et al., Anal. and Bioanal. Chem. **400**: 673-678, (2011).

[40] V. V. Maslyuk et al., App. Phys. A, Volume **94**, Issue 3, pp 485-489 (2009).

[41] S. Bhattacharjee et al., Chem. Phys. **377**: 96–99 (2010).

[42] V. Yu. Aristov et al., J. Chem. Phys. **128**, 034703 (2008).

[43] R. M. Dreizler, E. K. U. Gross, Density Functional Theory-An approach to the Quantum Many-Body Problem, Springer-Verlag Berlin Heidelberg, 1990

[44]F. Reinert, J. Phys.: Condens. Matter **15**: S693–S705 (2003).

[45] Sydney G. Davison, Maria Stęślicka, Basic Theory of Surface States, Clarendon Press, 1992.

[46] E. Bertel, M. Donath, World Scientific Pub Co Inc, (1994)

[47] A. Damascelli web page: http://www.phas.ubc.ca/~quantmat/ARPES.html

[48] S.D.Kevan et al., Phys. Rev. B **36**: 11 (1987).

[49] S. LaShell et al., Phys. Rev. Lett. **77**: 16 (1996).

[50] J. Henk et al., Phys. Rev. B **68**: 165416 (2003).

[51] J. Henk et al., J. Phys.: Condens. Matter **16**: 7581-7597 (2004).

[52] F. Reinert et al., Phys. Rev. B **63**: 115415 (2001).

[53] P. B. Corkum, Phys. Rev. Lett. **71**: 143903 (1993).

[54] C. Grazioli et al., Rev. Sci. Instrum. **85**, 023104 (2014).

[55] Titanium sublimation pump:
https://en.wikipedia.org/wiki/Titanium_sublimation_pump

[56] Scienta R3000: http://www.scientaomicron.com/en/products/357/1206

[57] M.Pedio, private communication.

[58] T. Ivanova et al., Jour.of Electr. Spectr. and Rel. Phenom. **156–158**: 200–203 (2007).